Citizen science supporting agricultural monitoring with hundreds of low-cost sensors in comparison to remote sensing data

Corbari, Chiara; Paciolla, N.; Ben Charfi, I.; Skokovic, D.; Sobrino, J. A.; Woods, M.

DOI:
10.1080/22797254.2022.2084643

Publication date:
2022

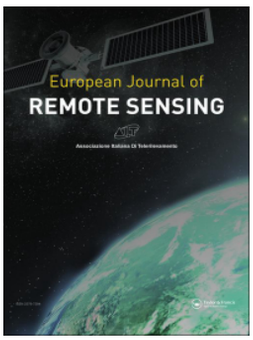

European Journal of Remote Sensing

ISSN: (Print) (Online) Journal homepage: https://www.tandfonline.com/loi/tejr20

Citizen science supporting agricultural monitoring with hundreds of low-cost sensors in comparison to remote sensing data

Chiara Corbari, N. Paciolla, I. Ben Charfi, D. Skokovic, J.A. Sobrino & M. Woods

To cite this article: Chiara Corbari, N. Paciolla, I. Ben Charfi, D. Skokovic, J.A. Sobrino & M. Woods (2022) Citizen science supporting agricultural monitoring with hundreds of low-cost sensors in comparison to remote sensing data, European Journal of Remote Sensing, 55:1, 388-408, DOI: 10.1080/22797254.2022.2084643

To link to this article: https://doi.org/10.1080/22797254.2022.2084643

Published online: 13 Jun 2022.

EUROPEAN JOURNAL OF REMOTE SENSING
2022, VOL. 55, NO. 1, 388–408
https://doi.org/10.1080/22797254.2022.2084643

Taylor & Francis
Taylor & Francis Group

RESEARCH ARTICLE

OPEN ACCESS Check for updates

Citizen science supporting agricultural monitoring with hundreds of low-cost sensors in comparison to remote sensing data

Chiara Corbari[a], N. Paciolla[a], I. Ben Charfi[a], D. Skokovic[b], J.A. Sobrino[b] and M. Woods[c]

[a]Department of Civil and Environmental engineering, Politecnico di Milano, Milan, Italy; [b]Image Processing Laboratory (IPL), University of Valencia, Valencia, Spain; [c]Duncan of Jordanstone College of Art & Design, University of Dundee, Dundee, UK

ABSTRACT

The ever-increasing importance of irrigation monitoring and water-use optimization in agriculture calls for new solutions for a more complete understanding of the plant growth dynamic and the agricultural water cycle. In this study, the fitness for use of the Flower Power low-cost sensors, not designed for scientific applications, is evaluated in an integrated agricultural monitoring context in contrast to freely available satellite information from Landsat 8, Sentinel 1 and 2. Measurements of air temperature, solar radiation, leaf area index (LAI) and soil moisture are considered. 456 sensors have been deployed in the Capitanata Irrigation Consortium (Italy) as part of the GROW Observatory project with local farmers collaborating as citizen scientists to either deploy these sensors, monitor the environmental variables and control irrigation management. The main results are: (i) positive agreement between Flower Power sensors and high-quality professional stations for measurements of meteorological variables (5.6°C RMSE for Air Temperature); (ii) acceptable estimates of crops LAI (RMSE = 0.55 m^2 m^{-2}) and mixed ones of Surface Soil Moisture (m = 0.75, R^2 = 0.23) from Flower Power sensors in respect to different satellite data; (iii) potentiality of these sensors combined with remote sensing in providing suitable tools for irrigation management.

ARTICLE HISTORY
Received 4 February 2022
Revised 30 April 2022
Accepted 27 May 2022

KEYWORDS
Multiple remote sensing data; citizen science; low-cost sensors; soil moisture; irrigation water needs

Introduction

Agriculture is the largest water user with about 70% of total freshwater consumption, which is projected to further increase due to climate change, population growth but also more demanding lifestyles and diets (Alexandratos & Bruinsma, 2012). Indeed, the average irrigation for a crop season in some regions can be at least twice the amount of rainfall (Kenawy & McCabe, 2016). Irrigated areas, although being about 2% of the global land area (17% of cultivated area) (Food and Agriculture Organization of the United Nations and (FAO), 2016), alter the land water cycle by locally increasing evapotranspiration and soil moisture, as infiltration and at catchment scale modifying the groundwater recharge and greatly reducing runoff, especially the peaks (Oki & Kanae, 2006).

Soil moisture information is then of fundamental importance for irrigation monitoring as well as for improving water management and irrigation efficiency. This may be achieved by combining ground (Choi et al., 2016; Ramadan et al., 2018) and satellite information with hydrological and crop models. For example, Phillips et al. (2014) analyzed ground measured and modelled soil moisture data at field scale for improving a decision support system; while Allen et al. (1998) computes the crops water requirements based on a crop coefficient. Calera Belmonte et al. (2005) improves this method by using satellite information for improving the crop coefficient definition and thus the evapotranspiration. Corbari et al. (2019) merged an energy-water balance model with meteorological forecast for irrigation scheduling. These models should be considered with their own limitations and potentialities, related mainly to ground sensors unavailability over large areas (Doraiswamy et al., 2004), or satellite data algorithms validation (Bastiaanssen & Bos, 1999) as for agro-hydrological models which usually need many parameters (Dong & Zhao, 2019; Sun & Ren, 2014).

A high spatial resolution of water distribution is then needed to achieve a sustainable data-driven management of water resources and this may be achieved with alternative methods for data collection (Barker et al., 2020; Mishra & Coulibaly, 2009; Ochoa-Tocachi et al., 2018), as well as for hydrological and agronomic models (Corbari et al., 2020).

Usually, traditional long-term hydrological monitoring networks are quite expensive in terms of instrumentations as well as maintenance by expert technicians (Mazzoleni et al., 2017; Mishra & Coulibaly, 2009), leading to few and sparse in time and space data collection. Remote sensing data are more and more available, but still limited by their spatial and temporal resolution or by the accuracy of the algorithms for variables retrievals (Bauer-Marschallinger et al., 2019; Skokovic et al., 2017a).

CONTACT Chiara Corbari chiara.corbari@polimi.it Politecnico di Milano, Piazza Leonardo da Vinci 32, Milan 20133, Italy

The involvement of citizens as scientists is then a possibility to enlarge the monitoring networks to gain new scientific knowledge on the water cycle and related ecosystem services (Ajates et al., 2020), based on low-cost instruments that can therefore be handled in large quantities and are in turn easy to use (Hadj-Hammou et al., 2017), allowing increasing social involvement. In the last years, many citizen science activities have grown covering different topics of environmental monitoring from abiotic environment (Pocock et al., 2017), climate monitoring (Gharesifard et al., 2017), as well as river flood risk management (Ferri et al., 2020). However, the quality and reliability of the data collected by these citizen observatories is an open issue for scientific use while a comprehensive analysis is missing leading to some concerns in the acceptance in the research community (Freitag et al., 2016). For agricultural monitoring, fewer applications are available referring in particular to soil moisture monitoring and other related variable as surface air temperature (AT) or radiation (Aragó Galindo et al., 2012; Michels et al., 2020; Vellidis et al., 2016).

The International Soil Moisture Network (ISMN, https://ismn.geo.tuwien.ac.at/) (W. A. Dorigo et al., 2011; W. Dorigo et al., 2021) is trying to overcome these limitations by collecting and harmonizing the available SM measurements globally from both traditional networks as citizen science ones. Remote sensing data could help in enlarging the soil moisture knowledge globally, while addressing different issues related to spatial and temporal resolutions, sensing techniques and retrieval algorithms accuracy or soil depth. In fact, active microwave sensors can reach 1 km of spatial resolution, as Sentinel1 data, but with the low temporal resolution of at least only four days (Bauer-Marschallinger et al., 2019), leading to the possibility of missing irrigation or rainfall events; while on the contrary passive microwave data, as SMOS or SMAP, have a daily revisit time but with a low spatial resolution of about 25 km (Entekhabi et al., 2014; Kerr et al., 2010). Active data on the contrary may pose different challenges related to the effect on the retrieval algorithms of complex roughness and vegetation backscatter on vegetated areas, which could be relevant in irrigated crops areas. So that ground soil moisture sensors are therefore fundamental for satellite calibration and validation.

Another important parameter in agricultural monitoring is the vegetation growth and its status. This may be monitored with the Leaf area index (LAI), which is the total green leaf area over the pixel area, and it's a critical parameter which is regulating the plant photosynthesis and respiration (Watson, 1947). This may be measured by traditional ground sampling based on time consuming and expensive field campaigns with direct (from harvested leaves) (Bréda, 2003) or indirect methods based on empirical relationships with, for example, tree diameters (Gower et al., 1999), or with canopy gap fraction according to the Beer-Lambert law (Nilson, 1971). LAI might also be monitored by remote sensing data usually through empirical algorithms with canopy reflectance or vegetation indices (VIs; Fang et al., 2019; Gower et al., 1999; Zucaro 2014), with the main change of the non-general relationship between LAI and reflectance for all vegetation types leading to some uncertainties (Garrigues et al., 2008).

The main objective of this paper is to evaluate the performances of low-cost sensors not designed for scientific use, the Flower Power (Parrot, https://www.parrot.com/), for an integrated agricultural monitoring, in respect to freely available satellite information. Specific sub-objectives are also identified: (i) to evaluate the agreement among ground meteorological measurements of air temperature (AT) and incoming shortwave radiation (Rs) from the Flower Power and high-quality professional stations, (ii) to evaluate the possibility to infer crops LAI from covered Flower Power sensors and compared against satellite LAI estimates, (iii) to compute the agreement and accuracy of soil moisture data from both Flower Power sensors and satellite Sentinel-1, (iv) to infer potential and actual evapotranspiration (ETP and ET, respectively), (v) to evaluate the suitability for irrigation management, computing the irrigation water needs (IWN) and irrigation deficit (ID).

This builds upon the GROW Observatory (GROW), a community-based environmental monitoring and information system, (GROW; https://growobservatory.org/), whose sensors network was deployed at scale in focus areas, identified as GROW Places, across Europe. Its aims were threefold, to validate and scale a meet a key scientific objective to ground-truth Sentinel 1 products using in-situ crowdsourced soil moisture data, to take a participant-cent ered approach to monitor soil and land in collaboration with citizens, and for empowered citizens and scientists to take up these data and insights achieve a more sustainable agriculture (Ajates et al., 2020; Woods et al., 2020). In particular, the 456 sensors deployed in the GROW Place at Capitanata Irrigation Consortium in South of Italy during July to October 2019, as part of the GROW Observatory, will be analyzed.

Materials

Capitanata area

The Capitanata Irrigation Consortium, specifically the Sud Fortore district, is located in Southern Italy in the Puglia region (Figure 1) and it is an intensive cultivated area, mainly devoted to durum wheat and tomatoes during the spring-summer season and fresh

vegetables in winter. It covers an area of about 65′000 hectares of which only 45% is irrigated through the Consortium water distribution network (56,700 ha), while the remaining areas are irrigated with private wells (INEA,). The role of irrigation is crucial in fact the mean irrigation volume for the irrigation season from April to October is about 600 mm, while the seasonal rainfall precipitation amount to 150 mm. Daily irrigation volumes measured in the main aqueduct are available from 2013 to 2018 and are provided by the Capitanata Irrigation consortium. During the different years, the volumes range over the whole season between 6 and 4.6 10^7 m^3 with a mean value of 5.3 10^7 m^3.

Low cost sensors

456 Flower Power low-cost on-ground sensors have been deployed in different fields either with bare soil or vegetation covered: mainly with tomatoes and asparagus but also with Cabbage, Celery, Fennel, Pak-Choi, Salad, Spinach. In Figure 1, the locations of the sensors are shown in the different fields and farms, along with the land cover of Autumn crops (mostly vegetated area). Two main groups of sensors can be identified and named Azienda and Onoranza, according to farmers naming. In fact, different farmers have been involved as citizen scientists to either deploy these sensors, monitor the environmental variables and control irrigation management.

The instruments are Flower Power from the French company Parrot SA, (https://support.parrot.com/us/support/products/parrot-flower-power), which are able to measure time series data collected at 15-minutes intervals: soil moisture (SM) (m^3 m^{-3}, at a maximum depth of 5 cm), air temperature (°C, few centimetres above ground surface) and solar illuminance (lux, measured in proximity of the air temperature sensor). The sensors characteristics are reported in details in Table 1. In particular, soil moisture is measured with a capacitance probe with two rods of 10 cm, which allows measuring the dielectric permittivity that is influenced by SM. Soil moisture accuracy has been tested through laboratory experiments by Xaver et al. (2020) showing a good accuracy of the sensors, except that for dry conditions of silty clay soils. Light intensity is measured by a sensor in the wavelength spectrum between 400 and 700 nm. The thermometer is positioned inside the plastic cover of the sensor. The data are stored on the Flower Power sensors and then downloaded by smartphones App via Bluetooth. In Figure 1, a picture of a Flower Power sensor is shown. Each sensor costs about 70 euro.

Data has been collected from the Parrot sensors which were deployed to gather continuous data between 22 July and 20 October 2019 (91 days). Among the 456 sensors, 69 were not operational due to lack of Bluetooth connection signal, discharged batteries after few hours or sensor breakage due to agricultural operations in the fields with tractors. Among the remaining 387 effectively active sensors during this monitoring period, the data collection was intermittent. Two major periods without any data can be identified in early August and in the first half of September, as detailed in Figure 2a. This lack of data is referable to the method of saving data on the internal memory of the sensor or to the data transfer between the sensor and the cloud database (e.g. this issue was not known a priori) For the other days, the average number of sensors collecting data was 102. Evaluating the data wealth for each sensor (Figure 2b), the average number of days with data for a given sensor was 18. A non-negligible number of sensors (76 sensors, or 20% of the active ones)

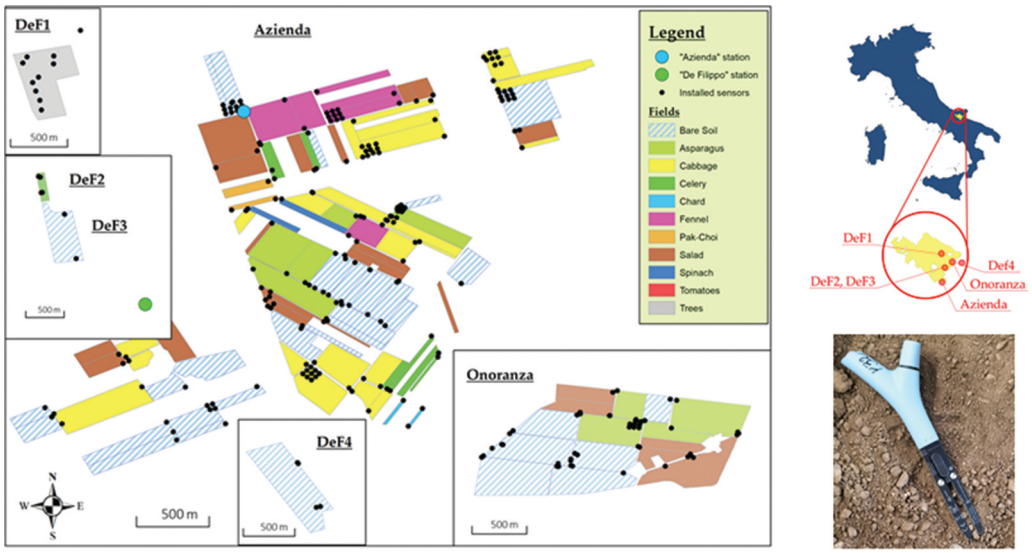

Figure 1. Capitanata Irrigation Consortium area within Italy. The autumn crop types and the installed sensors distribution are detailed in the different farms.

Table 1. Flower power and Davis measurements characteristics.

	Variable	Units	Range	Accuracy
Parrot	Air temperature	°C	−5 to +50°C	1.5°C
	Light intensity	Lux	0.1 to 200 lux	15%
	Soil moisture	Vol %	0 to 50%	3%
Davis	Air temperature	C	−40 to + 65°C	0.1°C
	Solar radiation	W m^{-2}	0 to 1800 W/m^2	1 W/m^2
	Rainfall	mm	0 to 6553 mm	0.2 mm

provided data for only one day, and a considerable group (158 sensors, 41% of the active ones) provided at most 20 days with data. The most prolific sensor was D363, placed in a Celery field in the DEF2 sector, with 61 days-worth of data.

In Figure 3, sensors distribution among the different fields is detailed. Two main surveys classified the different fields, one in July (at the start of the monitoring) and the other in October (at the end). The predominance of bare-soil fields is testified by the high amount of Bare Soil (BS) sensors in the July classification. Most of these, however, were part of a vegetated field by October. Tomato sensors, on the other hand, were the only group to shift from a vegetated field to a bare-soil one during Summer, because of the tomato harvest in August. The sensors installed in the vegetated fields are positioned in such a way that the measurement of illuminance is not influenced by the presence of the plant itself and at the same time some sensors are positioned under the crop's foliage, so that the perceived illuminance is influenced by the shade of the plant. Davis meteorological station.

Meteorological data were also available from 2 meteorological stations located in a 10 km range from the Flower Power sensors (Figure 1). The stations are Davis Vantage Pro2 Plus (https://www.davisinstruments.com/) equipped to measure air temperature (°C) and relative air humidity (%) at 2 m height (as standard WMO), incoming shortwave solar radiation (Wm^{-2}). The data accuracy and measurements range are reported in Table 1. The data were available every five minutes for all the monitoring period.

Remote sensing data

Vegetation indices

Data linked to vegetation were extracted by the use of Visible Near Infrared and Shortwave Infrared bands of Landsat8 and Sentinel2 satellites, to infer different vegetation indices (VIs). Concretely, the bands near to 660 nm and 850 nm were used for vegetation index estimation and bands near to 1600 nm and 850 nm for vegetation water content. All bands were atmospherically corrected by the use of 6S software (Vermote et al., 1997) in order to estimate the surface reflectance.

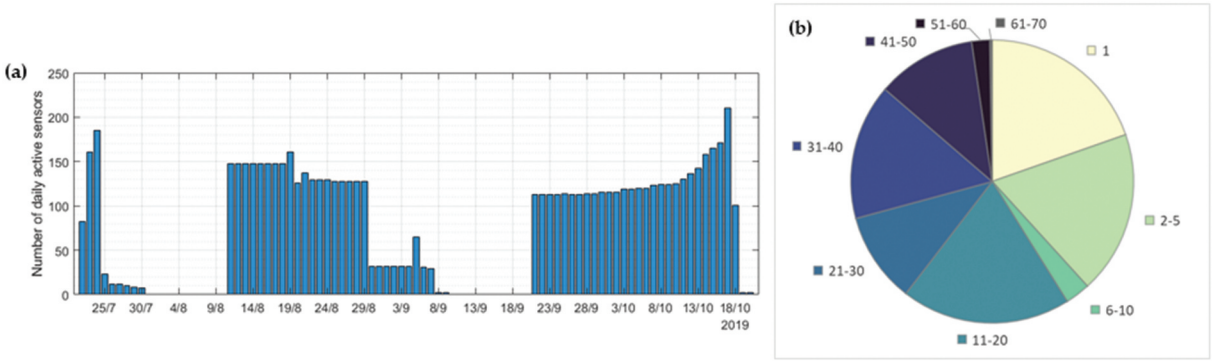

Figure 2. Number of active sensors for each day of the monitoring period (a). Sensors classified by number of days with data (b).

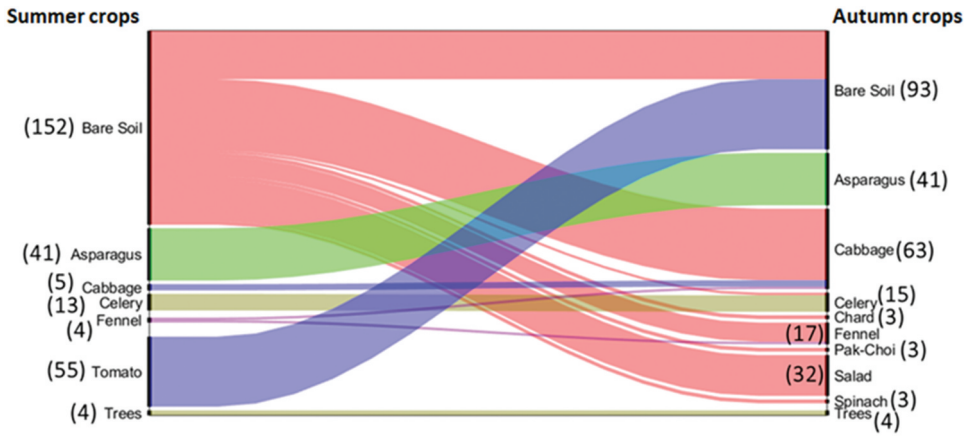

Figure 3. Sensors distribution among the crop type categories in the July and October patterns.

The Fractional Vegetation Cover (Fcover) identifies the fraction of the total pixel that is covered by the vegetation and can be estimated through NDVI, according to Gutman and Ignatov (1998), as:

$$\text{Fcover} = \frac{\text{NDVI} - \text{NDVI}_S}{\text{NDVI}_V - \text{NDVI}_S} \quad (1)$$

where NDVIs and NDVIv are representative NDVI values for bare soil and green vegetation pixels, respectively. These values were estimated as 0.15 and 0.9, respectively, based on images NDVI histograms. With Fcover, LAI can be calculated as (Choudhury, 1987):

$$\text{LAI} = -\frac{\ln(1 - \text{Fcover})}{k(\varphi)} \quad (2)$$

where k is the light extinction coefficient for a given solar zenith angle (φ). The light extinction coefficient is a measure of attenuation of radiation in the canopy which, in our case, it was set equal to 0.5.

Additionally, to NDVI, Soil Adjusted Vegetation Index (SAVI) was also computed in this work in order to reduce the soil background effect (Huete, 1988).

$$\text{SAVI} = \left(\frac{b_{850} - b_{660}}{b_{850} + b_{660} + L}\right)(1 + L) \quad (3)$$

where the sub-index of b refers to bands wavelength, in nanometers, and L accounts for first-order soil background variations and in our case is computed as the average vegetation cover of the image which vary from 1 (image full covered by vegetation pixels) to 0 (image full covered by bare soil pixels).

Moisture Stress Index (MSI) and Normalized Difference Water Index (NDWI) are two basic indices for estimation of vegetation water content. Equations for both are:

$$\text{MSI} = (b_{1600} - b_{850}) \quad (4)$$

$$\text{NDWI} = \frac{(b_{850} - b_{1600})}{(b_{850} + b_{1600})} \quad (5)$$

While the near infrared band is nearly unaffected by changing water content, shortwave infrared band reflectance increases or decreases with the decrease or increase of water leaves content, respectively.

Soil moisture

Soil moisture data (5–7 cm soil depth) were obtained at 1 km spatial resolution from the Copernicus product of Surface Soil Moisture Version 1 product (SSM1km) retrieved from Sentinel-1 C-band SAR backscatter after geo-correction and radiometric calibration (Bauer-Marschallinger et al., 2018). The output product is an index in percent of saturation, with 1°/112 nominal resolution. Overpasses from the Sentinel-1 are programmed every day, but the revisit time is longer, being in the case study area of about 3–4 days. A number of 26 images were available during the study period (20 July–20 October 2019). The data, provided in the form of saturation percentage, were converted to volumetric ratio (same unit as the Parrot SM) employing the known saturation and residual water content values for the area.

Land surface temperature

LST can be calculated through different techniques, which require the use of one, two or more thermal bands of one sensor. In our case, two techniques have been used: Single Channel (SC) algorithm and Split Window (SW) algorithm that were applied to Landsat-7 Enhanced Thematic Mapper Plus (ETM+) and Landsat-8 Thermal InfraRed Sensor (TIRS). For ETM+ and TIRS, LST has been retrieved following the procedure explained in Skokovic et al. (2017a) for SC algorithm and Jimenez-Munoz et al. (2014) for SW algorithm, respectively. The SC equation follows as:

$$T_s = \frac{T_{sen}^2}{b_\gamma L_{sen}}\left[\frac{1}{\varepsilon}(\Psi_1 L_{sen} + \Psi_2) + \Psi_3\right] + T_{sen} - \frac{T_{sen}^2}{b_\gamma} \quad (6)$$

where T_{sen} is the at-sensor brightness temperature, T_s is the LST, ε is the emissivity, b_γ is equal to 1277 K, and Ψ_1, Ψ_2 and Ψ_3 are related to the atmospheric parameters of transmissivity and upward and downward radiances.

The SW equation used for TIRS bands is presented as:

$$T_S = T_i + a_0 - a_1(T_i - T_j) + a_2(T_i - T_j)^2 + (a_3 + a_4 w)(1 - \varepsilon) + (a_5 + a_6 w)\Delta\varepsilon \quad (7)$$

where T_i and T_j are the at-sensor brightness temperatures at the SW bands i and j, ε is the average emissivity of I and j, $\Delta\varepsilon$ is the difference, w is the total atmospheric water vapor content ($g \cdot cm^{-2}$) and a_0, a_1, a_2, a_3, a_4, a_5 and a_6 are the SW coefficients with values of 16.40, −0.268, 1.378, 0.183, 54.30, −2.238 and −129.20, respectively.

For both equations, the atmospheric parameters and water vapor content, required as inputs, were estimated by MODTRAN 5.0 radiative transfer code to a forecasted European Center for Medium-Range Weather Forecasts (ECMWF) atmospheric profiles included in the Sentinel-3 data. For the emissivity inputs, also required in both equations, NDVI Thresholds Method (NDVI-THM) has been applied following the original equations presented in Sobrino et al. (2008). Finally, in order to disaggregate the ETM + and TIRS pixels from its original spatial resolution of 60 m and 100 m, respectively, to a resolution of 30 m, the Nearest Neighbour Temperature Sharpening (NNTS) methodology has been used as it is described

in Skokovic (2017b). The whole procedure of LST retrieval at a spatial resolution of 30 m is described in Corbari et al. (2020).

Methods

The implemented methodology is divided in the different steps which might be grouped in verification analyses and operative irrigation management. The first group of activities includes: (1) retrieval of radiation data from Parrot sensors and its agreement with that measured by professional sensors, (2) estimates of leaf area index from Parrot sensors and agreement evaluation with satellite LAI, (3) agreement between Parrot measure of air temperature and comparison with both AT measured data from professional sensors and LST from satellite data, (4) comparison between Parrot soil moisture and satellite SM estimates. While the second group of analyses encompasses: (1) computation of potential and effective evapotranspiration, (2) estimates of the evapotranspiration water deficit and the crop irrigation water needs.

Retrieval robustness is quantified through the evaluation of the root mean square error (RMSE), which is computed as follows:

$$\mathrm{RMSE} = \sqrt{\frac{\sum_{i=1}^{n} (S_i - M_i)^2}{n}} \tag{8}$$

where S_i is the ith Parrot-measured variable, M_i is the ith measured variable by profession stations or satellite, n is the sample size. These statistical values are computed knowing that the lower the RMSE is, the lower the error. In addition, the linear regression between the S_i and M_i is also verified and the angular coefficient (m) and the coefficient of determination (R^2) are computed.

Each sensor provides the amount of solar radiation it receives in the form of illuminance, expressed in lux (lx = lumen m^{-2}). This parameter identifies the total luminous flux impacting on a surface per unit area. The conversion into a standard radiation term (expressed in W m^{-2}) is mediated through the luminosity function y (λ), which is a wavelength-weighted relation between Watts and Lumens that accounts for the human eye sensibility to different energy wavelengths. In particular, the human eye is most sensitive to monochromatic radiation at 555 nm, and is unable to perceive energy outside the bounds of the visible electromagnetic spectrum (380–400 nm up to 700–780 nm). This means that the Lumen-to-Watt (Lux-to-Watt/m^2) conversion is not stable across all the wavelengths of the visible spectrum, but shows a peak at 555 nm (where 1 Watt = 683 Lumens) and has proportionally lower values for other wavelengths. The Lumen-to-Watt conversion factor (χ) is obtained as follows:

$$\chi = \varphi \int_0^{\infty} y(\lambda)\Gamma(\lambda)d\lambda \tag{9}$$

Where φ is the peak-sensitivity conversion coefficient (683 lm/W) and Γ(λ) is the relative solar radiative spectrum, normalized over the whole short-wave energy. The luminosity function data for the analysis has been elaborated by the Commission Internationale de l'Eclairage (CIE; Sliney, 2007) and the solar spectrum data is the Air Mass (AM1.5) G173 Global Tilt data from the American Society for Testing of Materials (ASTM). This procedure, following in the footsteps of Michael et al. (2020), provides a conversion factor of 116 lx to 1 W/m^2.

Before applying this conversion to the whole dataset, a more empirical approach has been taken. Illuminance data has been compared with shortwave radiation measurements from the standard Davis meteorological station. This comparison has been restricted with two conditions: only non-cloudy days, classified according to the information from the meteorological station, are considered, and nocturnal data, identified by the sensors minima (0.1 lx for the Parrot sensors and 0 W m^{-2} for the Davis station), are excluded. From this comparison, an illuminance-to-radiation conversion coefficient can be obtained, with varying results among all the sensors. The comparison of such empirically-retrieved information with the theoretically correct approach described above will be also discussed.

Leaf area index

By establishing a comparison between contemporary measurements of illuminance from sensors in vegetated and bare-soil fields, a dampening ratio can be obtained. As the vegetation shadow reduces the perceived illuminance, this ratio is strictly correlated to the Leaf Area Index parameter. According to the theory of Campbell and Norman (1998), the dampening ratio of the solar radiation (and, by extension, of the illuminance) has been directly linked to the leaf density in the arboreal medium through the expression:

$$\mathrm{LAI} = -\frac{\ln\left(\frac{I_{veg}}{I_{bare}}\right)}{K(\varphi)} \tag{10}$$

$$K(\varphi) \stackrel{def}{=} \frac{\sqrt{x^2 + \tan(\varphi)^2}}{x + 1.774(x + 1.182)^{-0.733}} \tag{11}$$

Where I_{veg} identifies the solar illuminance for a vegetated sensor and I_{bare} the same parameter for a bare-soil sensor. The beam extinction coefficient K depends on the solar zenith angle (**φ**) and the leaf spatial distribution index (x). The latter is a parameter accounting for the presence of any preferential

direction for the leaves spatial distribution: a unitary value indicates a spherical (thus isotropic) distribution, with no preferential directions. The computed Leaf Area Index is defined as the one-faced green leaf area per unit ground area, directly connected to leaf density.

Effective and potential evapotranspiration

The potential evapotranspiration has been computed according to the general micro-meteorological conditions of the area, using the meteorological data measured from the Parrot sensors as well as gathered from the Davis station in place. The Priestley–Taylor equation (Priestley & Taylor, 1972) was used:

$$\mathrm{ETP} = 1.3\frac{\Delta}{(\Delta+\gamma)}\mathrm{R_S} \tag{12}$$

where ETP is in mm, $\Delta = \mathrm{d}(e_{sat})/\mathrm{dT}$ (Pa K^{-1}), which is the slope of the curve relating saturated water vapor pressure e_{sat} (Pa) to temperature T (°C), γ (Pa K^{-1}) is the psychrometric constant, Rs is the incoming shortwave radiation (W m^{-2}).

The actual evapotranspiration has then been obtained by constraining the potential evapotranspiration with the soil moisture availability of each single field. ET is computed by multiplying the ETP for a reduction coefficient: the β and α functions for vegetated and bare-soil fields, respectively. In particular, the β function (Kutílek & Nielsen, 1994) is based on the concept that when the soil moisture value is lower than the field capacity (FC), the vegetation stoma begins to close and transpiration decreases significantly, until it stops completely for soil moisture values less than or equal to the wilting point (WP). The equation is:

$$\beta(\mathrm{SM}) = \begin{cases} 0, & for \quad SM \le WP \\ \frac{\mathrm{SM}-\mathrm{WP}}{\mathrm{FC}-\mathrm{WP}}, & for \quad WP < SM < FC \\ 1, & for \quad SM \ge FC \end{cases} \tag{13}$$

The α function for bare-soil fields is expressed as (Parlange et al., 1999):

$$\alpha = 0.082 \cdot \mathrm{SM} + 9.173 \cdot \mathrm{SM}^2 - 9.815 \cdot \mathrm{SM}^3 \tag{14}$$

Irrigation water needs and irrigation deficit

Two operational products for irrigation management have finally been developed from the data gathered by the sensors.

The irrigation deficit (ID) was computed portraying the amount of water required by the plants to transpire at full potential. This ID can be computed for each sensor by evaluating the potential to actual evapotranspiration deficit:

$$\mathrm{ID} = \mathrm{ETP} - \mathrm{ET} \tag{15}$$

The irrigation water needs (IWN) for each specific crop were evaluated according to a crop stress threshold (stress), defined following the methodology of Allen et al. (1998) in the FAO-56 paper. This stress threshold might be used as an indication of a correct or excessive irrigation but also, if available in real-time application, to trigger irrigation. The threshold was computed considering the different crop types and the soil characteristics, as:

$$stress\ threshold = \mathrm{FC} - \mathrm{p} \cdot (\mathrm{FC} - \mathrm{WP}) \tag{16}$$

where p is a reduction coefficient depending on the crop and climatic parameters. p is defined by Allen et al. (1998) for several crops (http://www.fao.org/3/x0490e/x0490e00.htm#Contents). The factor p normally varies from 0.30 for shallow rooted plants at high rates of ET (> 8 mm d^{-1}) to 0.70 for deep rooted plants at low rates of ET (< 3 mm d^{-1}). A value of 0.50 for p is commonly used for many crops. The p factor is usually corrected for climatic data (Allen et al., 1998).

Results

Air temperature

The air temperature measurements collected by the sensors have been compared with those of the Davis stations, associating each sensor to the nearest station. An example is shown in Figure 4. Sensor G222 (Figure 4a) is placed in a permanently-bare soil field. The Parrot air temperature (PAT), although similar to the station air temperature (SAT) in the nocturnal hours, attains much higher values during the day, reaching temperatures 10–15°C warmer. The main reason for this may be the measurement height: while PAT is collected a few centimetres above ground, SAT is measured 2 metres above ground. This means that, although conceptually different, PAT has much in common with satellite land surface temperature, which is displayed in the same Figure 4, even though displaying higher values especially in the summer. Another issue could be the overheating of the plastic cover of the sensor, as pointed out by Xaver et al. (2020). Other three sensors are displayed, with different behaviors. Sensor GO190 (Figure 4b) is in a Tomato field: the shadow from the plants causes the PAT to be much closer to the SAT during August; after the harvest, the PAT measured in the now-bare field grows again higher than SAT. Sensor D363 (Figure 4c) displays an opposite trend. Placed in a Celery field, the PAT values display the bare-soil trend during summer, when the crop is still virtually nonexistent; as it grows, PAT converges to SAT under the influence of vegetation. Finally, Sensor G150 (Figure 4d), placed in an Asparagus field, shows a more regular trend, similar to that of the bare-soil

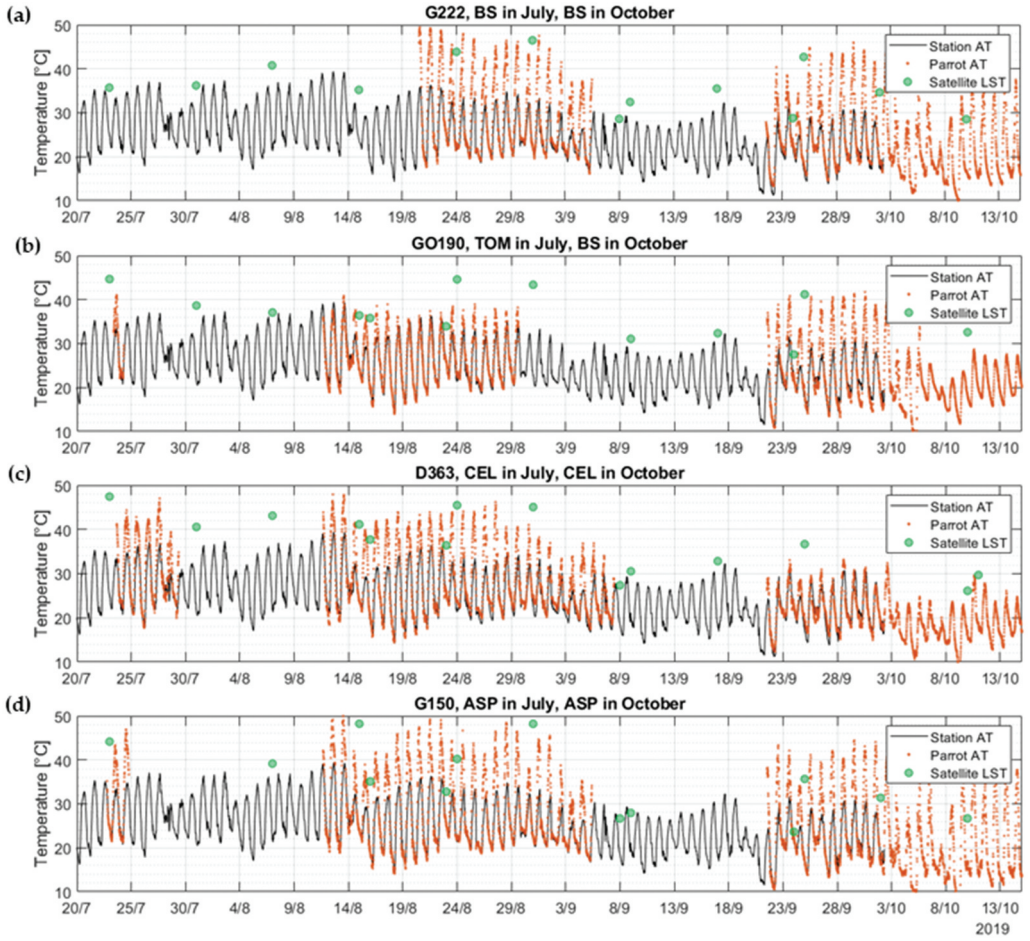

Figure 4. Time series of air temperature from Parrot sensors (Orange dots) and Davis station (black line), together with land surface temperature from Landsat 7 and 8 satellites (green circles). BS is bare soil, TOM tomatoes, CEL celery, ASP is asparagus.

sensor (Figure 4a). This can be motivated by the scarce vegetation density of the Asparagus crop, that poorly affects the downwelling radiation.

To understand the general behavior, all the sensors data were compared with both the Davis station air temperature (Figure 5a) and the high-resolution (30 m) LST data retrieved from Landsat 7 and 8 (Figure 5b). The comparison was done considering data every 15 minutes, with the Davis stations data are averaged at this frequency from their original sampling time of 5 minutes. This provides a high number of PAT-SAT couples (402,487) and, for a better representation, the scatterplot has been replaced by a density plot. The PAT overestimation already discussed for Figure 4 is clearly visible in the right-hand side of the density plot. Accounting for all PAT-SAT couples, the PAT overestimation can on average be set at +78%, although the moderate regression coefficient ($R^2 = 0.78$) displays the wide variety of different behaviors among the sensors. Isolating nighttime sampled data, the fitting between the two datasets improves consistently ($R^2 = 0.80$ and $m = 0.91$).

Figure 5b identifies the comparison between PATs and satellite LST. In this case, the satellite overpass time (around 11:25 a.m.) is a major constraint, reducing the number of PAT-LST couples to 1017. There appears to be a certain correlation between the two datasets, as shown by the close-to-one slope coefficient of the interpolation ($m = 1.02$). However, the data seems poorly clustered around the interpolation line, as testified by the moderate R^2 value (0.44).

To try and discern the specifics of this comparison, sensors were divided according to the vegetation type. The sensor-to-satellite coupling statistics are detailed in Table 2. As a reference, the sample dimension (number of sensor-to-satellite couplings) is also shown. Focusing on the most numerous crop types, bare soil, celery and tomatoes provide, on average, a negative sensor-to-satellite bias, while asparagus, fennel and trees show a positive bias. However, as the correlation coefficients show, no category overcomes the 0.5 mark, indicating a high sample dispersion.

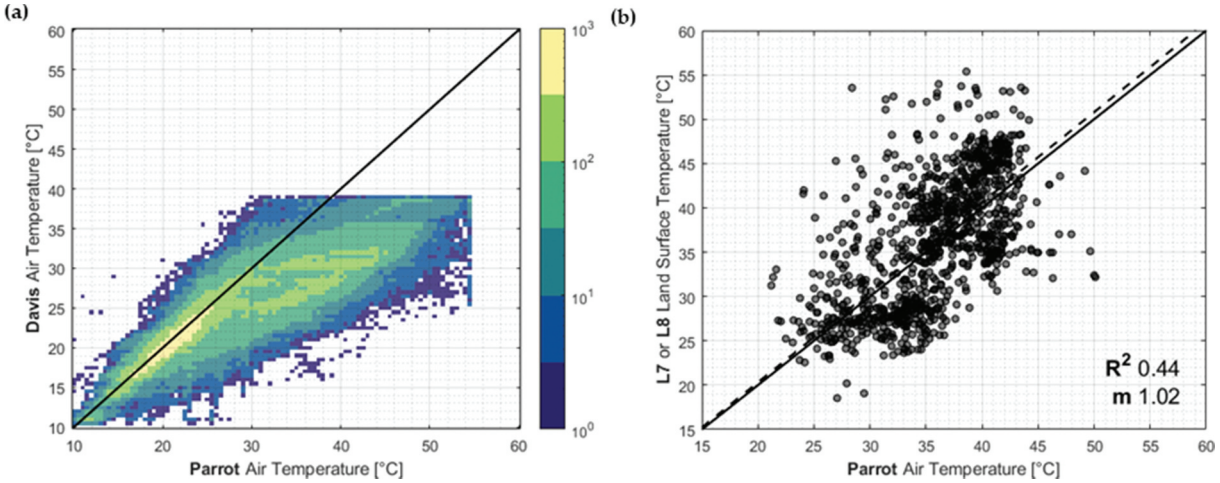

Figure 5. Comparison between Parrot air temperature (PAT) and station air temperature (SAT) (a) or Landsat 7/8 land surface temperature (LST) (b).

Radiation

The comparison between the converted Parrot in incoming shortwave solar radiation with the shortwave radiation from the Davis Station, in order to be meaningful, has been regulated removing three data categories: cloudy days data, data from sensors under the vegetation and nocturnal data. An example of this comparison is provided in Figure 6a for Sensor G67, placed in a bare soil field. The resulting conversion coefficient (m = 5.69), obtained with a strong accuracy (R^2 = 0.96), is a characteristic of this particular sensor. In fact, other sensors show similar values, although each specific to its own data.

The wide variety of illuminance-to-radiation couplings is mapped in Figure 6b. The black diagonal line identifies the 5:1 ratio between radiation and illuminance, with most of the sensors crowding the area immediately above, as suggested by the 5.41 average value. Another great group is the one on the left-hand side of the plot, with very low illuminance values corresponding to high radiation values collected by the station. These

Table 2. Correlation information for the sensor-to-satellite couplings sorted by crop type.

Crop	Couples	R^2	Avg. Bias	Crop	Couples	R^2	Avg. Bias
All sensors	1017	0.44	−0.7°C	Celery	60	0.46	−1.4°C
Bare Soil	551	0.45	−0.4°C	Fennel	24	0.48	+0.1°C
Asparagus	165	0.44	+1.1°C	Tomato	179	0.39	−3.4°C
Cabbage	7	0.20	−0.9°C	Trees	15	0.32	+1.4°C

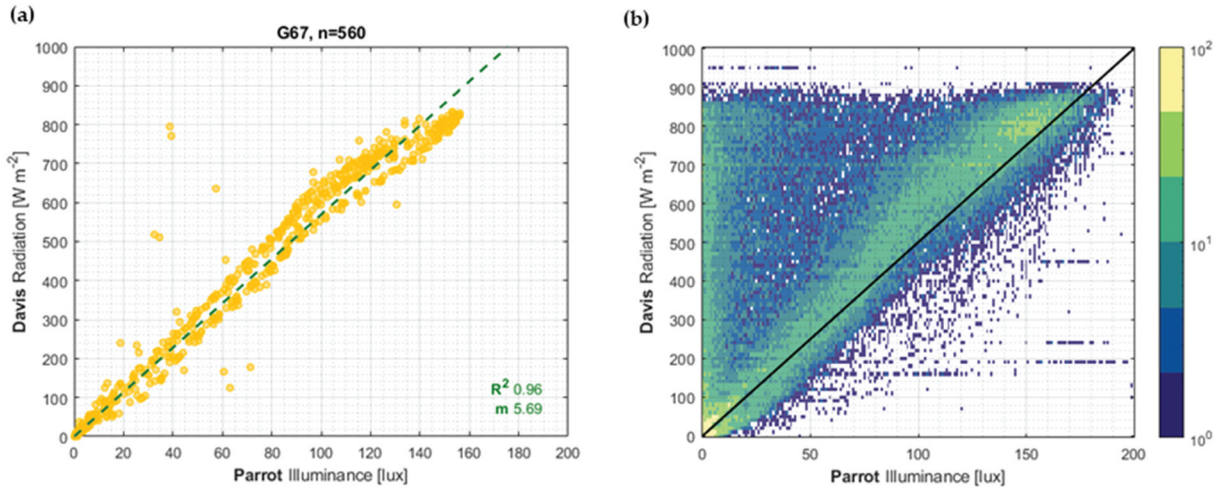

Figure 6. Sensor-to-Station comparison between illuminance and radiation. Example on a bare soil sensor (a) and global density plot for all the sensors (b).

couplings are mainly referred to vegetated sensors, where the dampening effect differentiates the two parameters. Among the 110 sensors providing suitable data for the comparison, the average conversion coefficient is 5.41, with a low variation coefficient (6.4%). These conversion values (5.41 W/m^2 to 1 lux) are quite different from the 116 lux to 1 W/m^2 theoretically expected (Michael et al., 2020). However, if the peak-sensitivity conversion coefficient φ of Eq. 8 is neglected, re-adjusting that equation provides a final conversion coefficient equal to the solution of the integral, that is, 5.91 lux to 1 W/m^2, which is quite close to what has been found empirically. This suggests that what is displayed by the Flower Power sensor, more than "actual" solar illuminance, is rather "peak-corrected" incoming radiation, obtained from the actual illuminance using only the peak-sensitivity coefficient and neglecting the role of the luminosity function.

Leaf area index estimates

Leaf area index, as obtained following the procedure detailed in Section 3.2, were compared against estimates from Sentinel 2 satellite data. Contrasting results in term of agreement are found. Figure 7a shows a good correlation with a positive trend, as the field is shifting from an empty bare soil to a vegetated pattern (cabbage). This evolution is evident both in the sensor and satellite retrievals, both in general trend and in actual LAI values. On the contrary, Figure 7b provides as example the results for sensor GO186 with an opposite negative behavior, due to its positioning in an asparagus field, with a reduction of the vegetation coverage in the monitoring period. The general decreasing satellite LAI trend and its actual values result well-interpreted by the sensor.

On the other hand, Figure 8 displays two examples of the satellite-sensor comparison with a low correlation. Figure 8a involves another sensor (G71) placed in an asparagus field: but while the sensor registers LAI values around 1 m^2 m^{-2}, its corresponding satellite pixel featured practically null values (0.019 m^2 m^{-2} at most). Looking more in details the LAI satellite image (Figure 8b), it clearly appears how the Parrot sensor placement, in the angle of the asparagus field, creates a conflict with its covering pixel. In fact, the sensor shares the pixel space with the neighbouring, mainly bare soil area, affecting the overall LAI value. As a reference, the neighbouring pixel (just 9 m west of the sensor) has been added to the plot in Figure 8a, showing a LAI series much more in tune with that obtained from the sensor. The same concept applies for sensor G122 (Figure 8c), placed in an originally bare soil field, later cultivated with celery. Also in this case, the sensor-to-satellite divergence is due to the fact that the sensor has been placed to the corner of the crop field and, once again, the neighboring satellite pixel shows a LAI time series more in line with what the sensor perceives.

Overall, isolating the sensors without field-border problems such as those detailed above, the agreement between sensor and satellite is acceptable, with a low average RMSE value (0.55 m^2 m^{-2}) and varying performances across the sensors (R^2 = 0.34).

Soil moisture measurements

Comparison with SM satellite data

The whole Parrot SM dataset was compared against satellite data obtained associating each sensor to the Copernicus SSM1km product pixel, nominally 1 km^2 large. In the first panel of Figure 9, the overall scatterplot, involving all sensors, is shown. Although the interpolation slope is not far from unity (m = 0.75), it is clear how the heterogeneity of each Copernicus cells clashes with the degree of detail provided by the Parrot sensors (R^2 = 0.23). In the other panels of Figure 9, the same data is provided filtered out by land cover, starting from the bare soil category and covering all crops found in the area. The correspondence varies a lot from category to category with m values ranging between 0.84 for the bare soil field to 0.50 for chard crops, confirming

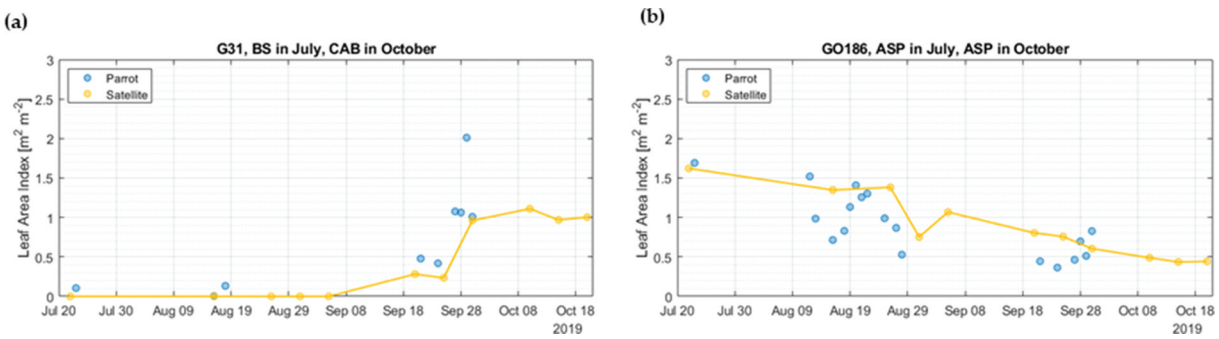

Figure 7. Two examples of successful comparison between sensor-computed LAI and data gathered from satellite. BS is bare soil, CAB cabbage, ASP is Asparagus.

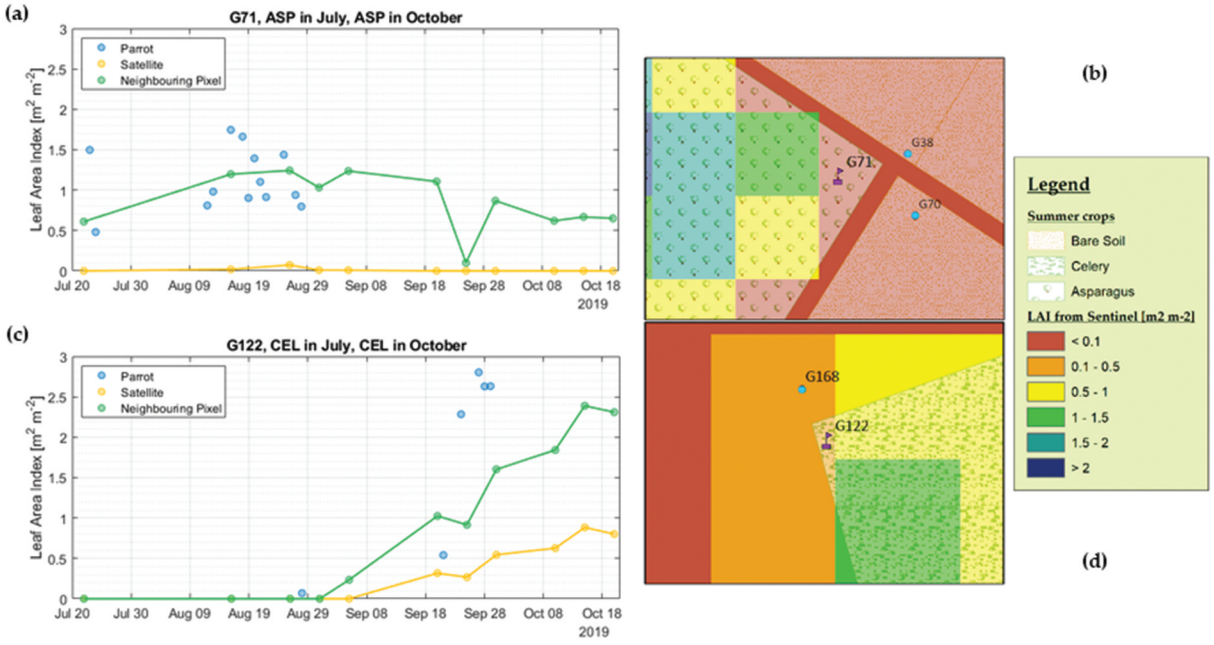

Figure 8. Two examples of problematic comparison between sensor-computed LAI and data gathered from satellite: (a) and (b) for an asparagus (ASP) sensor the time series and the map, (c) and (d) for a celery (CEL) field.

the difficulties of microwave radar data in retrieving soil moisture in highly vegetated fields (Giacomelli et al., 1995). Low values of R^2, never higher than 0.31, are obtained for all the fields.

To better understand also the spatial resolution issue of the satellite images, in Figure 10, one of the Copernicus SM1km pixels has been selected for a focus, as it covers 56 different Parrot sensors over the total period of observation. The time series of Copernicus SM, completed by the dataset uncertainty in the shaded area, is shown in Figure 10a together with the SM distribution of all the active Parrot sensors in the same pixel. A similar behavior in the overall trend is observable among the two datasets detecting the SM increases for the rainfall events, while high differences in the absolute values are detected, showing a RMSE of 0.116, a slope of the interpolation line of 0.76 with a R^2 of 0.12. This may be explained by the different land cover conditions of the considered satellite pixel (July, Figure 10b and October, Figure 10c) of the observation period, which describe a particularly bare pixel.

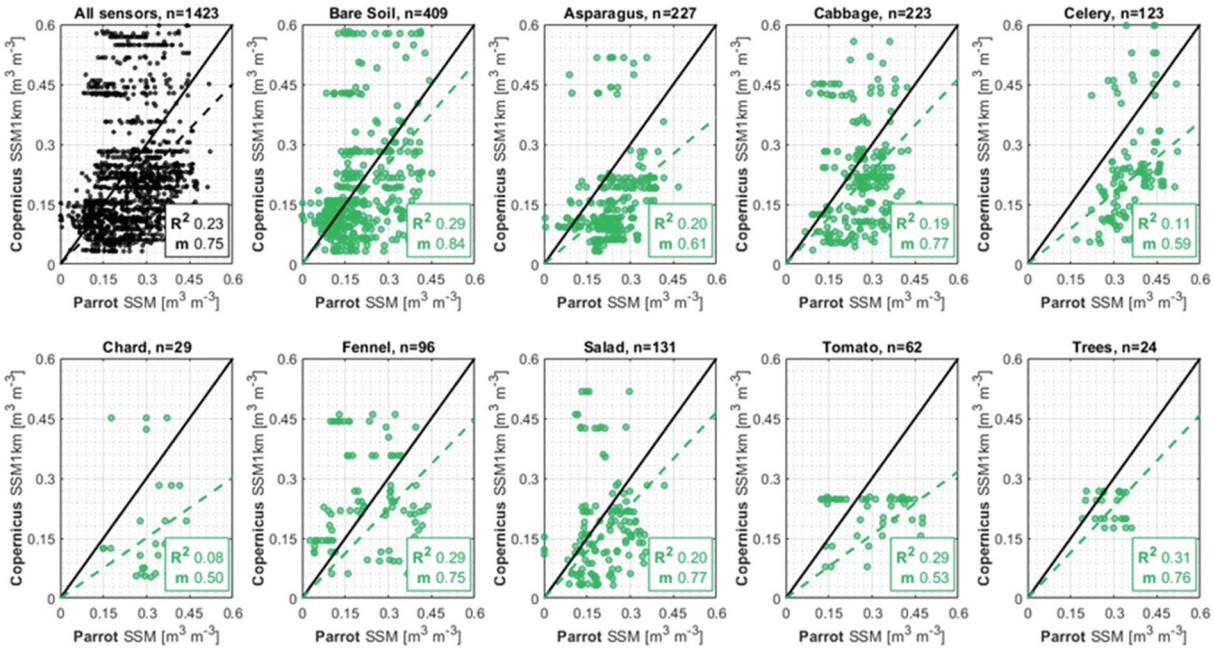

Figure 9. Parrot to Copernicus soil moisture comparison for different crops categories. Number of couples (n), determination coefficient (R^2) and interpolation slope (m) are provided for each plot.

Comparison with satellite water stress indices

Parrot soil moisture data were then compared to some satellite-derived vegetation indices, in order to ascertain their sensibility to soil moisture variations. To this aim, Fcover, MSAVI, MSI, NDVI, NDWI obtained from Sentinel 2 and Landsat 8 satellite images are compared with Parrot SM data at pixel scale. The comparison between sensors and vegetation indices is explored in detail for three different sensors in Figure 11, showing mainly that these indices seem to evolve with the crop status of the area. Sensor 8360 (Figure 11a), located in a celery field, sees a progressive increase in irrigation during summer to prepare the soil for the plant growth with high value of SM. All the VIs are progressively increasing as well with the crop development, but remain quite clustered around similar values. The same happens with an asparagus sensor (F070, Figure 11b) and a tomato one (849E, Figure 11c). The VIs do not show particularly sharp changes in low-SSM phases, corresponding to stress conditions for the crop. Generally, low temporal frequency in the VIs data is poorly compatible with the rhythms of plant water stress and irrigation for most crops, as can be seen particularly well for the celery and tomato sensors.

An overall analysis on the SM-VIs relation was performed through a cross-correlation between the different datasets, as shown in Table 3, considering all the Parrot sensors. The strong relation between the different VIs is evident in the high correlation (or anti-correlation, in the case of MSI) values, while all of them display a close-to-zero correlation against SM.

Effective and potential evapotranspiration

Even though the potential evapotranspiration has been computed, according to equation 11, using the radiation and air temperature data measured by each single sensor, similar ETP values were obtained from the different sensors with a quite small standard deviation of 1.1 mm day^{-1}. This consistent estimate of potential evapotranspiration is also visible in Figure 12, where a boxplot for each date was computed considering all available sensor each day. On each box, the central mark indicates the median, and the bottom and top edges of the box indicate the 25th and 75th percentiles, respectively. The whiskers extend to the most extreme data points not considered outliers, and the outliers are plotted individually using the "+" symbol. The ETP outliers may be linked to the possible uncertainties deriving from the conversion coefficient of lux data to incoming shortwave radiation, especially for those sensors partially covered from vegetation. The potential evapotranspiration seasonal trend is also visible showing decreasing values during the monitoring period according to climate behavior: high values of about 10 mm day^{-1} during August which decrease around 6 mm day^{-1} during the first half of October.

As expected, a higher variability is instead observable in the effective evapotranspiration computed from each Parrot sensors data, as being directly interconnected to the soil moisture dynamic following the rainfall and irrigation events. The time evolution of the two evapotranspiration estimates, effective and potential, are compared in Figure 13 for few sensors' examples covering different crop types dynamic, along with soil moisture data. The

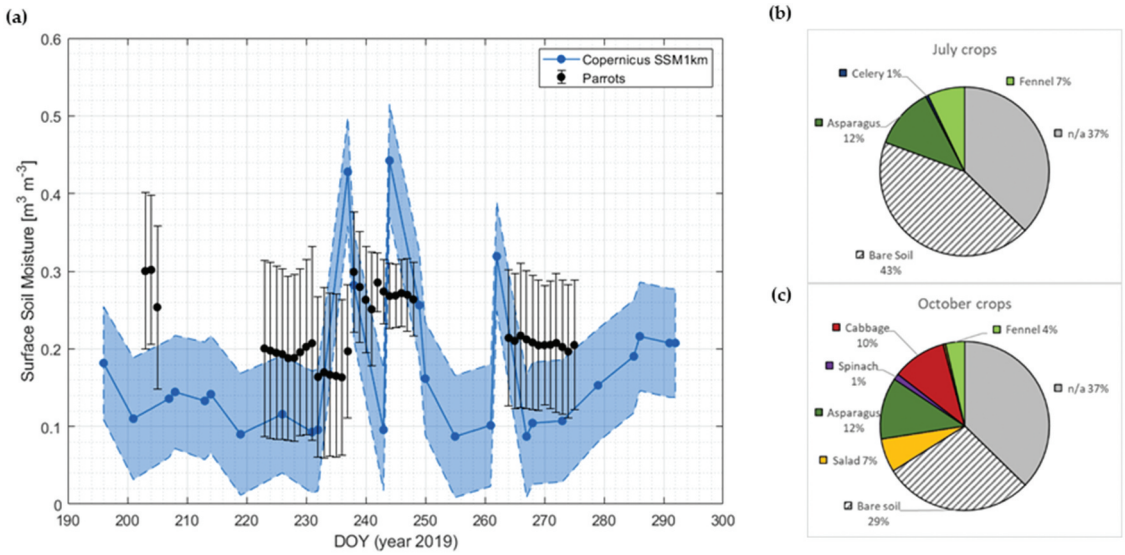

Figure 10. SM time series example for a Copernicus SSM1km pixel, with its uncertainty (shaded area) and the SM distribution of the Parrot sensors located within the pixel (a). July (b) and October (c) field type distribution is also detailed.

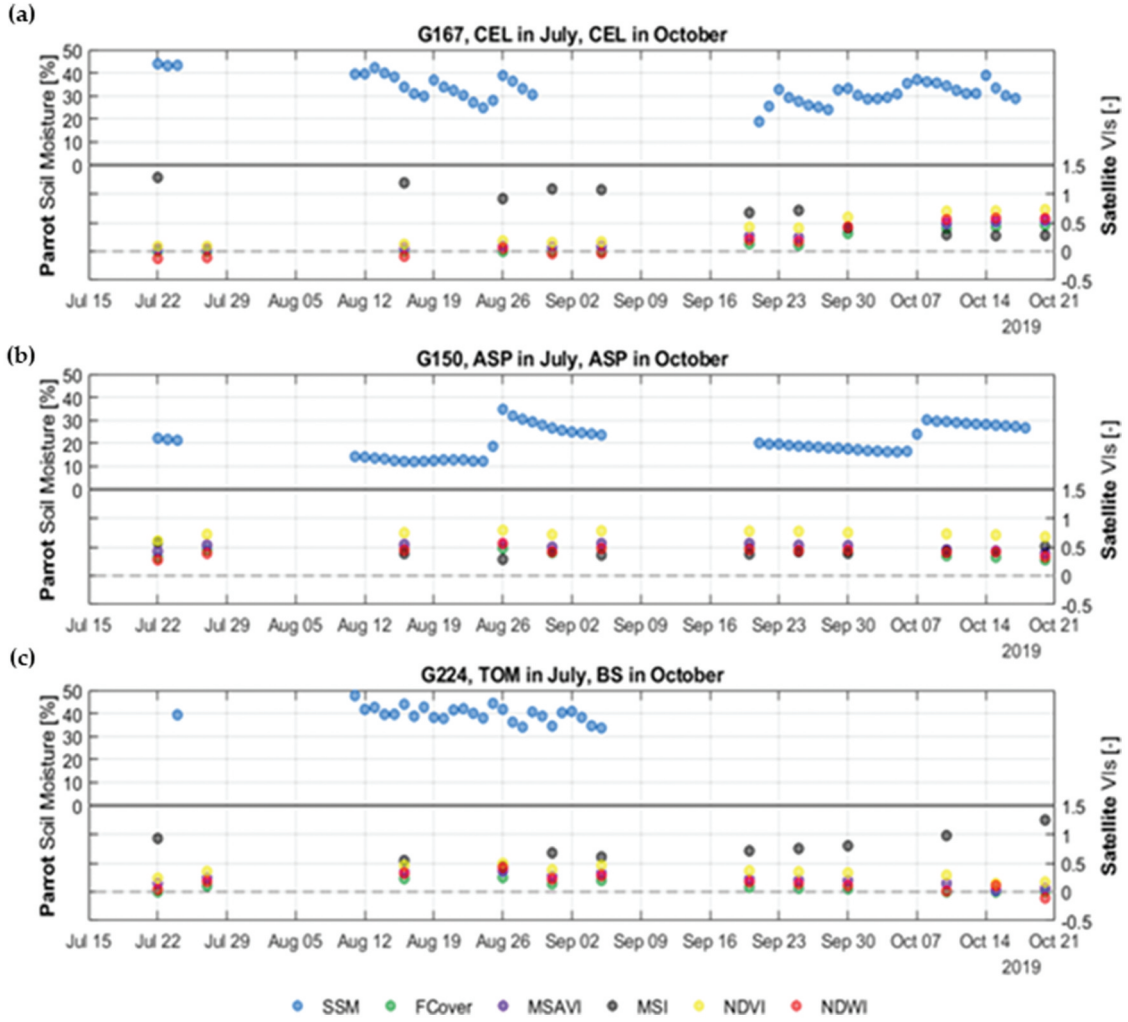

Figure 11. Time evolution of Parrot soil moisture (upper half) and satellite vegetation indices Fcover, MSAVI, MSI, NDVI and NDWI (VIs, lower half) for some selected sensors in the plots on the right: (a) celery field (CEL), (b) asparagus crop (ASP), (c) tomato crop (TOM) and bare soil (BS).

Table 3. Correlation coefficients between SM and the vegetation indices.

	SM				
Fcover	−0.03	Fcover			
MSAVI	−0.07	0.96	MSAVI		
MSI	−0.08	−0.84	−0.79	MSI	
NDVI	−0.09	0.91	0.88	−0.80	NDVI
NDWI	−0.07	0.83	0.83	0.97	0.84

upper panel (Figure 13a) identifies a sensor placed in a bare soil field during the whole analyzed period from July to October. The soil moisture values are always very low (lower than 0.1, except for the 26 of August during a precipitation event). This is reflected in the effective ET that is almost equal to zero. A similar behavior is observable in the second panel of Figure 13b where a sensor is located in a bare soil field during July while in the end of September spinaches have been sowed and hosting a fully-developed celery crop in October. By following the SM evolution, it is clear how a previously-empty field (SM values below wilting point at mid-August) is prepared for cultivation with insistent irrigation, until it transpires at full potential (SM well above the Field Capacity) by October. The third panel (Figure 13c) identifies a celery plot which undergoes harvesting during the monitoring period. The evapotranspiration is constantly equal to potential values for the cultivation period, with SM much higher than the field capacity. After harvesting, the field is left to dry, with a considerable decrease in SM. The last panel (Figure 13d) identifies a sensor placed in an Asparagus field. The oscillating pattern of the SM is reflected in the time behavior of the evapotranspiration. SM is generally oscillating around the field capacity leading to ET near its potential values.

Irrigation water needs

Two operational products have finally been developed for irrigation management purpose from the data gathered by the sensors.

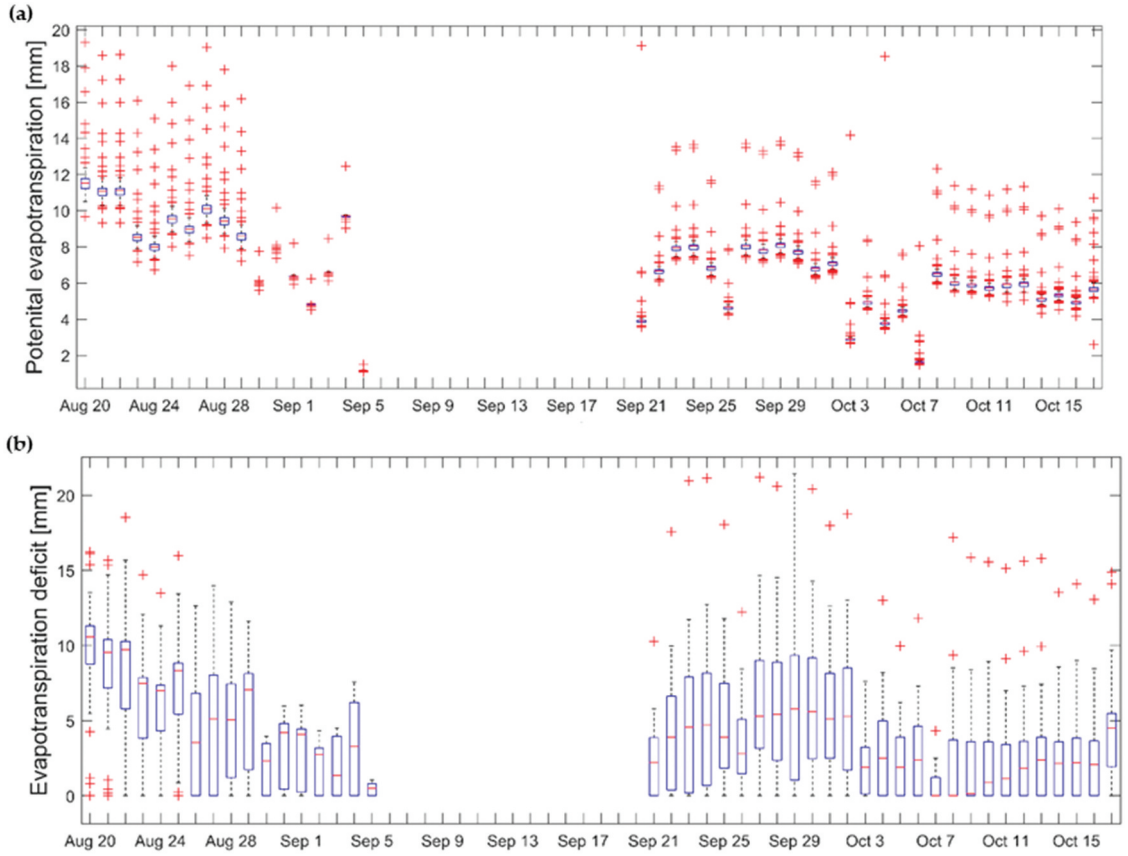

Figure 12. Box plot of the potential evapotranspiration (a) and the evapotranspiration deficit (b) for all the available sensors for each date.

Evapotranspiration based IWN

In particular, the irrigation deficit (ID), as the difference between potential and actual evapotranspiration, was computed at daily scale for each sensor. This indicator might help in understanding the amount of water required by the plants to transpire at full potential. In Figure 12b, a boxplot for each date was computed considering all available sensor each day. A higher deficit is observable during August with many plots being dryer, while during the month of October the different between ET and ETP is generally smaller due to soil moisture values near the field capacity threshold due to intense irrigation. A high intra-day variability is also observable, being the sensors installed in bare-soil fields and irrigated crops fields, which are in turn different crop types, at different growth stages and hence irrigated with different strategies.

Soil moisture based IWN

The second operative product for irrigation management was directly derived from the Parrot soil moisture data, in particular by comparing it against the crop stress threshold of each crop and the field capacity (Figure 14). In the upper panel (Figure 14a), a bare soil field with almost zero water into the soil is then planted with cabbages in the beginning of September. A typical soil moisture dynamic of an irrigated field is then observable with values oscillating between the stress threshold and well above the field capacity with an irrigation timing of about 5 days. This last SM behavior indicates an excessive irrigation volume. A similar behavior, but with an opposite timing, is visible for the second panel (Figure 14b), where the sensor 8C2C is located in a celery field during August. SM oscillates every 5 days between the stress threshold and well above the FC value. A precise irrigation amount is instead observable in the Asparagus field (sensor EBA6) with SM never exceeds the FC value during its oscillating dynamic with a 4 days amplitude, in the middle panel (Figure 14c). The lower panel (Figure 14d) refers to a bare soil field where soil moisture remains well below the wilting point threshold (except for the rainy event of 25–26 August) for all the monitored period, being the soil not irrigated.

The SM data from the Parrot sensors have then been compared with the SM Copernicus SSM1km in terms also of irrigation water needs. For the test date of 20 August 2019, the IWN has been computed both using the sensors data and the satellite retrievals. The Copernicus SSM1km pixel, covering an area around 74 ha, results coarser than the average field in the area (2.6 ha wide). This means that for a single satellite SSM value, numerous sensor SSM data are available. To this comparison, two Copernicus pixels have been selected, one covering the main Azienda area (in

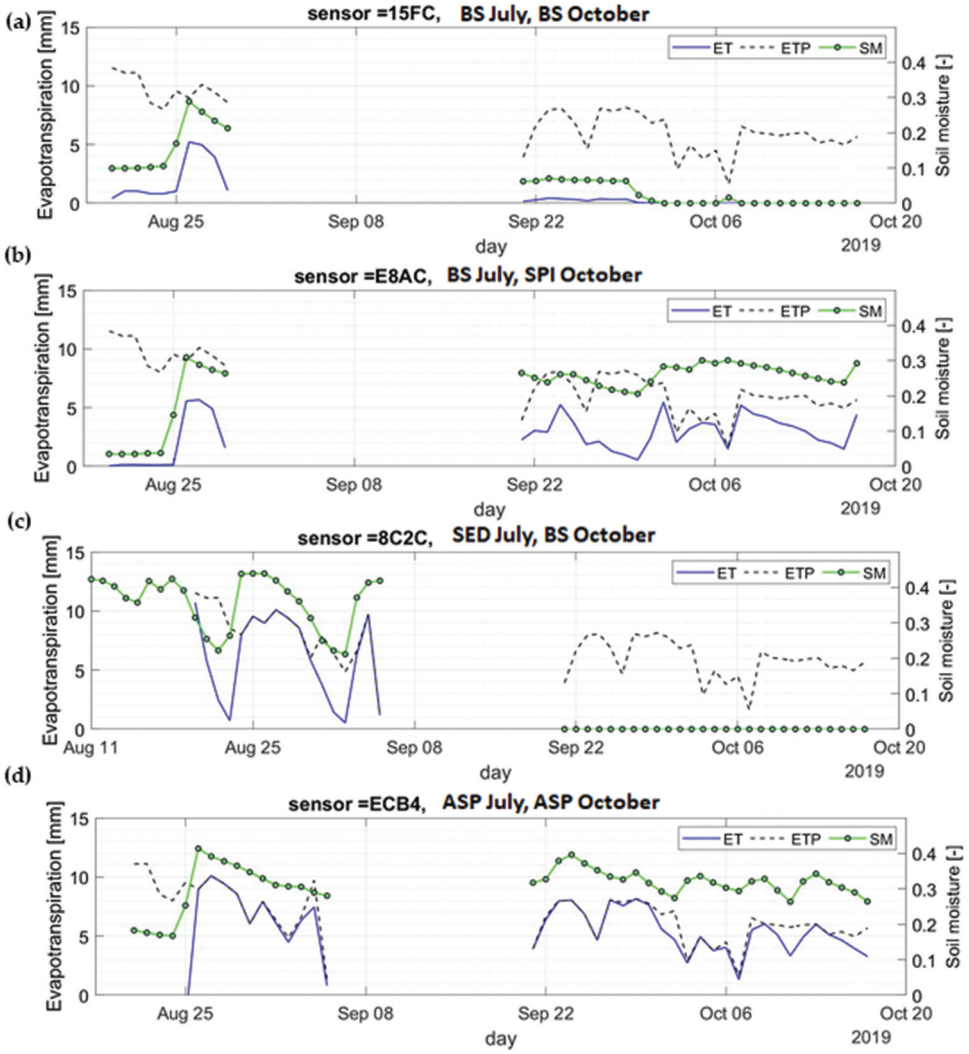

Figure 13. Four example computations of the ET and ETP linked to the soil moisture dynamic: a fully bare-soil field (BS) (a), a bare-soil (BS) plot being planted with spinach (SPI) (b), a vegetated plot (SED) being harvested (BS) (c), a continuously cultivated field with asparagus (ASP) (d).

which 54 sensors were active in the selected date) and the other in the Onoranza area (covering 11 sensors in the selected date). In Figure 15, the upper row shows the Azienda pixel, both in terms of actual SM (Figure 15a) and of IWN (Figure 15b). The sensor SM data have been classified in two distinct categories: irrigated areas (consisting of about 15% of the total pixel area for that date) and non-irrigated areas. The former includes all sensors associated with crops that are detected as irrigated from the Parrot sensors. In fact, the Parrot sensors located into the Asparagus fields sensors while being a cultivated field are associated to the second category of bare soil, since they are irrigated with sub-superficial drip irrigation at the depth of 20 cm is practically invisible to both the Parrot sensors, which have a sensing depth of ca. 7 cm, as well as to the Copernicus SSM (around 5 cm). For each sensor category, the average SM value is indicated with the bold red horizontal line, while for the irrigated areas sensors the FAO crop stress threshold is also displayed (dashed line) as a reference. The difference in behaviors among the Parrot sensors is evident. For both the Azienda and the Onoranza pixels, the low amount of irrigated areas (15% and 26%, respectively) mean that the Copernicus SSM is closer to the non-irrigated areas sensors, with values around the wilting point. In terms of IWN, as for both pixels the average sensor SM for the irrigated areas is higher than the field capacity, no irrigation is required; on the other hand, using Copernicus SSM would prompt important irrigation volumes (around 10 mm) (Figure 15b,d).

Discussion and conclusions

The potentiality of Citizen Observatories' such as GROW in the research context is a quite new topic, which is still to be fully analyzed and understood. Thanks to recent technological developments (Friha et al., 2021; Yang et al., 2021), IoT infrastructures have created new methods for data collection and interpretation (e.g. Wireless Sensor Networks, as the one analyzed in this study, but also Unmanned Aerial Systems and Agricultural Robotics) and smart agricultural

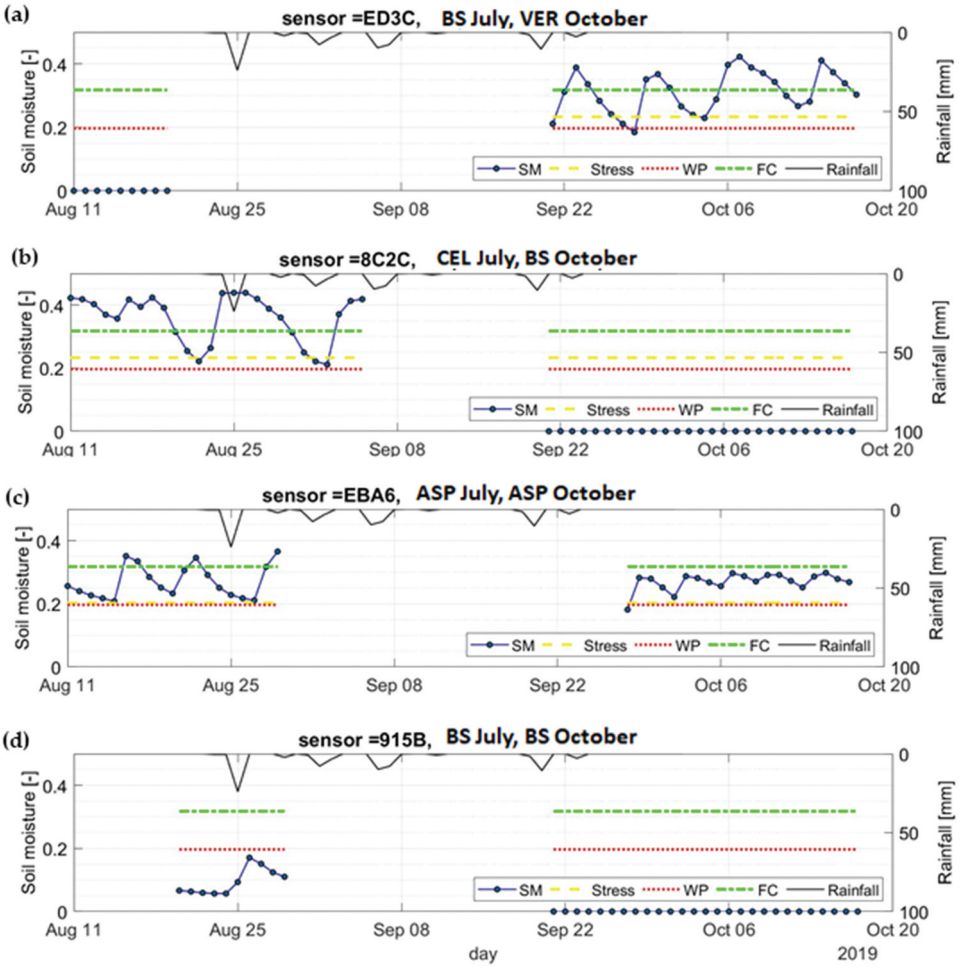

Figure 14. Four examples of soil moisture dynamic: a bare-soil (BS) plot being planted (SPI) (a), a vegetated (CEL) plot being harvested (BS) (b), a continuously cultivated field with asparagus (ASP) (c) a fully bare-soil field (BS) (d).

management (Angelopoulos et al., 2020). Their increasing, wide-ranging availability allows the involvement of a larger number of people and increases the opportunities for a sustainable management of water resources starting from the single citizen (Buytaert et al., 2014). The GROW citizen observatory has demonstrated the ability to actively involve and motivate a wide range of growers and farmers, from smallholders to big companies for improving water management in a sustainable way as well as the scientific community (Kovács et al., 2019; Woods et al., 2020).

However, currently in the scientific community there is no defined standard and accurate evaluation procedure to identify the value of using citizen science data. This "scientific education" question has also been recognized as one of the challenges that needs to be addressed in order to effectively enforce smart agriculture (Friha et al., 2021). In this paper, we analyzed the reliability of low-cost sensors for agricultural monitoring in respect to other traditional professional ground measurements and satellite information.

In the literature, numerous studies revolve around the management of low-cost sensing networks for smart agricultural management. Positive instances of development and use of such networks can be found in Tagarakis et al. (2021), who obtained good results in terms of independence and reliability in small to medium sized orchards, and in Panjabi et al. (2018), who conducted a reliable and accurate monitoring of a small agricultural watershed in Canada.

As a general result, the Flower Parrot sensors could be a valuable source of information that could be used to integrate traditional measures, especially thanks to their highly dense distribution in space. Nevertheless, each measured data must be analyzed with particular attention.

In fact, looking in more detail, Parrot air temperature has been found to be in agreement with professional air temperature data especially during the night (night-time RMSE of 1.6°C), while during the daytime hours and especially over bare soil fields higher discrepancies are obtained mainly due to the PAT measurement height of 5 cm and the overheating of the sensor plastic cover (daytime RMSE increases up to 7.7°C). In fact, daytime PAT has been proved to be higher correlated with satellite LST, with a close-to-one slope coefficient of the interpolation.

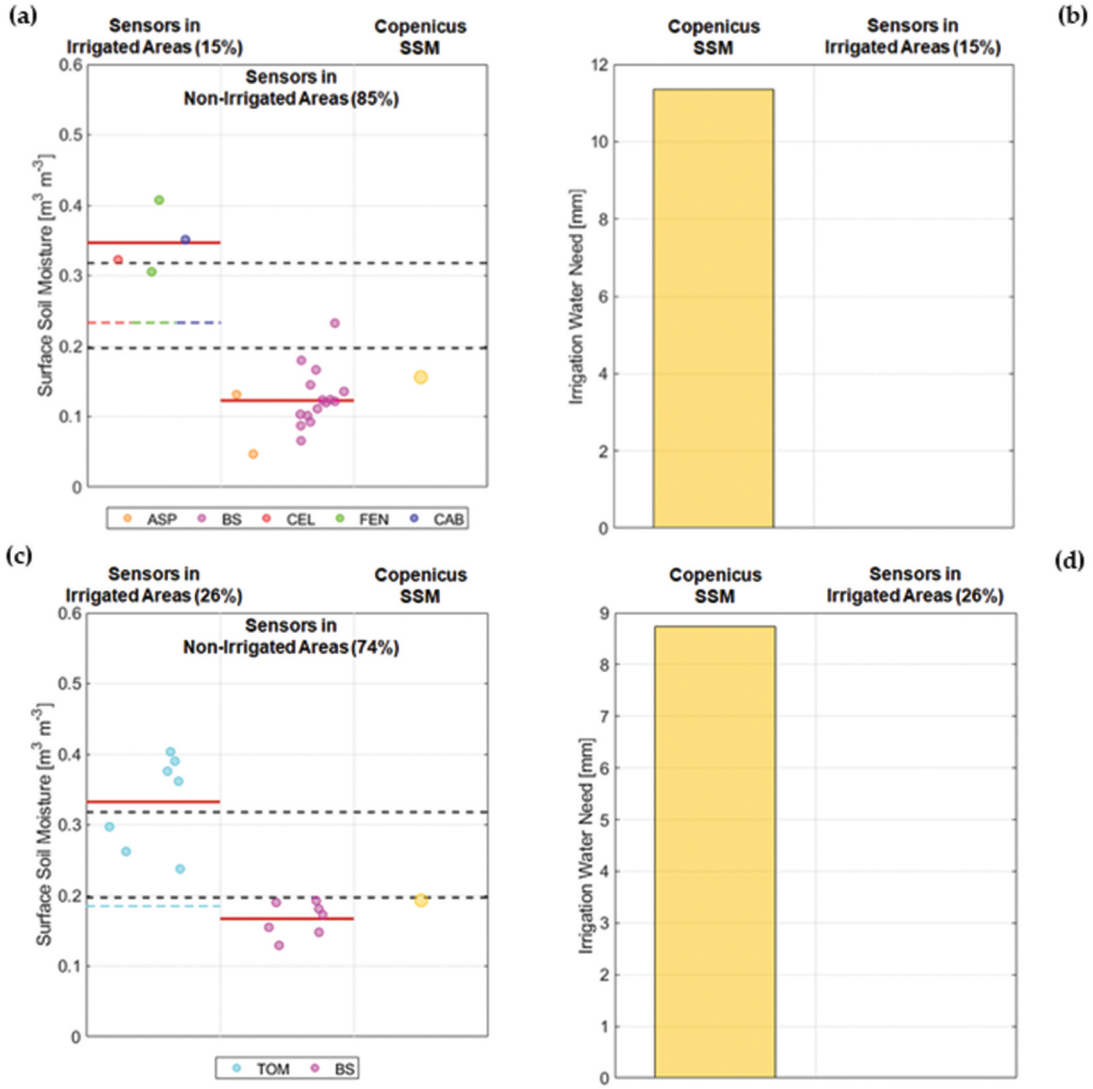

Figure 15. Soil moisture values from Parrot sensors and Copernicus SSM for the "Azienda" (a) and the "Onoranza" (c) selected pixels, for the 20 August 2019. Corresponding IWN are also shown, respectively, (b) and (d). ASP is asparagus, BS bare soil, CEL celery, FEN is fennels, CAB cabbage, TOM tomatoes.

A strong correlation has been obtained among the Flower Parrot sensors illuminance data and the incoming shortwave radiation data for all sensors. Among non-shadowed sensors, the conversion coefficients were detected around 5.41, with quite small dispersion (variation coefficient of 6.4%).

Acceptable results (RMSE = 0.55 m^2 m^{-2}, R^2 = 0.34) are obtained between the LAI estimated from the ground sensors and the remote sensing data, excluding the situations in which the sensor is located in a satellite pixel straddling several fields with different coverages.

A higher variability is instead obtained when the sensors' SM is compared with the Copernicus SSM1km data, which, due to its low spatial resolution, is not able to capture the variability detected by the ground measurements showing a low R^2 of 0.23 and a general underestimation (m = 0.75) caused by bare-soil fields. These results are in accordance with those obtained by Zappa et al. (2019) which showed that low-cost sensors are a valuable tool for satellite SM data validation over a more homogenous cover area. These Parrot SM data might be of great interest to improve the knowledge of soil moisture spatial variability, otherwise not detectable with the traditional sensors, as also reported by Bogena et al. (2010).

The sensors potentiality has been also demonstrated by computing the more operative agricultural monitoring indices, as the evapotranspiration deficit as well as the irrigation water needs based on the crops soil moisture stress thresholds providing higher variability in respect of using only a satellite image information.

A limitation of these Parrot SM data might be linked to the measurements depth which is limited to few centimeters which is less relevant to farmers to water the plants being the roots usually much deeper; while this depth corresponds to the sensitive area of Sentinel 1 signal allowing its comparison and validation (Zappa et al., 2019).

Besides measurement accuracy, another issue with the applicability of Parrot Flower Power sensors is related to their functioning reliability. In fact, out of the 456 sensors, 387 sensors provided data covering more than a couple of days with many data gaps, while only 158 sensors provided at most 20 days with data. Notably, no data was stored for the 31 July – 10 August and 8 September – 20 September periods due to sensors acquisition issues. Some sensors have also been lost during the end of August harvest operations.

The general quality of these data could also be affected by the bad use or installation by farmers, providing some results outliers in the acquired data. A proper merging of the information from a dense ground low-cost network with satellite information could be a good solution for improving irrigation management and agricultural monitoring activities, overcoming the problems of each specific type of data.

Acknowledgments

This work has been developed according to the Community Champion Organization Agreement of the GROW Observatory project funded by the European H2020 framework. Thanks to Pavlos Georgiadis, Mel Woods, Drew Hemment for managing the GROW Community and the project. A special thanks to Stefano and Paolo Guzzetti, Luigi Corbari from Guzzetti Farm, and to Giuseppe de Filippo e Pellegrino Riccio of Futuragri Farm for hosting the field measurements, and to Marco Mancini for the valuable discussions.

Author contributions

Chiara Corbari (CC), Nicola Paciolla (NP), Mel Woods (MW); Data curation: CC, NP, Imen Ben Charfi (IBC), Drazen Skokovic (DS); Formal analysis: CC, NP, DS; Project administration: MW; Supervision: CC, MW and Josè Sobrino (JS); Writing: all authors contributed to it.

Availability of data and material

The data are available at https://discovery.dundee.ac.uk/en/datasets/grow-soil-moisture-data

Code availability

Code is available upon request to the authors.

Disclosure statement

No potential conflict of interest was reported by the author(s).

Funding

This work was supported by the European H2020 [GROW Observatory project]; ERANETMED EU [RET-SIF project].

References

Ajates, R., Hager, G., Georgiadis, P., Coulson, S., Woods, M., & Hemment, D. (2020). Local action with global impact: The case of the GROW observatory and the sustainable development goals. *Sustainability*, *12*(24), 10518. https://doi.org/10.3390/su122410518

Alexandratos, N., & Bruinsma, J. (2012). World agriculture towards 2030/2050: The 2012 revision. ESA Working paper No. 12-03. Rome, FAO.

Allen, R. G., Pereira, L. S., Raes, D., & Smith, M. (1998). *Crop evapotranspiration—guidelines for computing crop water requirements* (pp. 300). Irrigation Drainage, FAO.

Angelopoulos, C. M., Filios, G., Nikoletseas, S., & Raptis, T. P. (2020). Keeping data at the edge of smart irrigation networks: A case study in strawberry greenhouses. *Computer Networks*, *167*, 107039 (pp.1-10). https://doi.org/10.1016/j.comnet.2019.107039

Aragó Galindo, P., Granell, C., Molin, P. G. & Huerta Guijarro, J. (2012). Participative site-specific agriculture analysis for smallholders. *Precision Agriculture*, *13*(5), 594–610. https://doi.org/10.1007/s11119-012-9267-4

Barker, J. B., Woldt, W. E., Wardlow, B. D., Neale, C. M., Maguire, M. S., Leavitt, B. C., & Heeren, D. M. (2020). Calibration of a common shortwave multispectral camera system for quantitative agricultural applications. *Precision Agriculture*, *21*(4), 922–935. https://doi.org/10.1007/s11119-019-09701-6

Bastiaanssen, W. G. M., & Bos, M. G. (1999). Irrigation performance indicators based on remotely sensed data: A review of literature. *Irrigation and Drainage System*, *13*(4), 291–311. https://doi.org/10.1023/A:1006355315251

Bauer-Marschallinger, B., Freeman, V., Cao, S., Paulik, C., Schaufler, S., Stachl, T., & Wagner, W. (2019). Toward global soil moisture monitoring with Sentinel-1: Harnessing assets and overcoming obstacles. *IEEE Transactions on Geoscience and Remote Sensing*, *57*(1), 520–539. https://doi.org/10.1109/TGRS.2018.2858004

Bogena, H., Herbst, M., Huisman, J., Rosenbaum, U., Weuthen, A., & Vereecken, H. (2010). Potential of wireless sensor networks for measuring soil water content variability. *Vadose Zone Journal*, *9*(4), 1002–1013. https://doi.org/10.2136/vzj2009.0173

Bréda, N. J. J. (2003). Ground-based measurements of leaf area index: A review of methods, instruments and current controversies. *Journal of Experimental Botany*, *54*(392), 2403–2417. https://doi.org/10.1093/jxb/erg263

Buytaert, W., Zulkafli, Z., Grainger, S., Acosta, L., Alemie, T. C., Bastiaensen, J., De Bièvre, B., Bhusal, J., Clark, J., Dewulf, A., Foggin, M., Hannah, D. M., Hergarten, C., Isaeva, A., Karpouzoglou, T., Pandeya, B., Paudel, D., Sharma, K., Steenhuis, T., , and Zhumanova, M. (2014). Citizen science in hydrology and water resources: Opportunities for knowledge generation, ecosystem service management, and sustainable development. *Frontiers in Earth Science*, *2*(26), 1–26. https://doi.org/10.3389/feart.2014.00026

Calera Belmonte, A., Jochum, A. M., Cuesta García, A., Montoro Rodríguez, A., & López Fuster, P. (2005). Irrigation management from space: Towards user-friendly products. *Irrigation and Drainage System*, *19*(3–4), 337–353. https://doi.org/10.1007/s10795-005-5197-x

Campbell, G. S., & Norman, J. M. (1998). *An introduction to environmental biophysics* (2nd ed.). Springer-Verlag. https://doi.org/10.1007/978-1-4612-1626-1

Choi, K. Y., Choi, E. Y., Kim, I. S., & Lee, Y. B. (2016). Improving water and fertilizer use efficiency during the production of strawberry in coir substrate hydroponics using a FDR sensor-automated irrigation system. *Horticulture, Environment, and Biotechnology*, *57*(5), 431–439. https://doi.org/10.1007/s13580-016-0072-2

Choudhury, B. J. (1987). Relationships between vegetation indices, radiation absorption, and net photosynthesis evaluated by a sensitivity analysis. *Remote Sensing of the Environment*, *22*(2), 209–233. https://doi.org/10.1016/0034-4257(87)90059-9

Corbari, C., Salerno, R., Ceppi, A., Telesca, V., & Mancini, M. (2019). Smart irrigation forecast using satellite LANDSAT data and meteo-hydrological modelling. *Agricultural and Water Management*, *212*, 283–294. https://doi.org/10.1016/j.agwat.2018.09.005

Corbari, C., Skokovic Jovanovic, D., Nardella, L., Sobrino, J., & Mancini, M. (2020). Evapotranspiration estimates at high spatial and temporal resolutions from an energy–water balance model and satellite data in the capitanata irrigation consortium. *Remote Sensing*, *12*(24), 4083. https://doi.org/10.3390/rs12244083

Dong, F. L., & Zhao, Y. Y. (2019)Irrigation scheduling optimization for cotton based on the aquacrop model. *Water Resources Management*, *33*, 39–55. https://doi.org/10.1007/s11269-018-2087-1

Doraiswamy, P., Hatfield, J., Jackson, T., Akhmedov, B., Prueger, J., & Stern, A. (2004). Crop condition and yield simulations using Landsat and MODIS. *Remote Sensing of the Environment*, *92*(4), 548–559. https://doi.org/10.1016/j.rse.2004.05.017

Dorigo, W. A., Wagner, W., Hohensinn, R., Hahn, S., Paulik, C., Xaver, A., Gruber, A., Drusch, M., Mecklenburg, S., van Oevelen, P., Robock, A., & Jackson, T. (2011). The international soil moisture network: A data hosting facility for global in situ soil moisture measurements. *Hydrology and Earth System Sciences*, *15*(5), 1675–1698. https://doi.org/10.5194/hess-15-1675-2011

Dorigo, W., Himmelbauer, I., Aberer, D., Schremmer, L., Petrakovic, I., Zappa, L., & Sabia, R (2021). The international soil moisture network: Serving earth system science for over a decade. *Hydrology and Earth System Sciences Discussion*. [preprint]. https://doi.org/10.5194/hess-2021-2, in review, 2021.

Entekhabi, D., Yueh, S., O'Neill, P. E., Kellogg, K. H., Allen, A., Bindlish, R., & Johnson, J. (2014). *SMAP handbook—soil moisture active passive—mapping soil moisture and freeze/thaw from space* (pp. 400–1567). (J. P. Laboratory, Ed.). JPL Publication.

Fang, H., Baret, F., Plummer, S., & Schaepman-Strub, G. (2019). An overview of global leaf area index (LAI): Methods, products, validation, and applications. *Reviews of Geophysics*, *57*(3), 739–799. https://doi.org/10.1029/2018RG000608

Ferri, M., Wehn, U., See, L., Monego, M., & Fritz, S. (2020). The value of citizen science for flood risk reduction: Cost–benefit analysis of a citizen observatory in the Brenta-Bacchiglione catchment. *Hydrology and Earth System Sciences*, *24*(12), 5781–5798. https://doi.org/10.5194/hess-24-5781-2020

Food and Agriculture Organization of the United Nations and (FAO). *Global Map of Irrigation Areas (GMIA)*. Available from: http://www.fao.org/nr/water/aquastat/irrigationmap/index.stm 2016

Freitag, A., Meyer, R., & Whiteman, L. (2016). Strategies employed by citizen science programs to increase the credibility of their data. *Citizen Science: Theory and Practice*, *1*(1), 2. https://doi.org/10.5334/cstp.6

Friha, O., Ferrag, M. A., Shu, L., Maglaras, L., & Wang, X. C. (2021). Internet of things for the future of smart agriculture: A comprehensive survey of emerging technologies. *IEEE/CAA J. Autom. Sinica*, *8*(4), 718–752. https://doi:.org/10.1109/JAS.2021.1003925

Garrigues, S., Lacaze, R., Baret, F., Morisette, J. T., Weiss, M., Nickeson, J. E., Fernandes, R., Plummer, S., Shabanov, N. V., Myneni, R. B., Knyazikhin, Y., & Yang, W. (2008). Validation and intercomparison of global leaf area index products derived from remote sensing data. *Journal of Geophysical Research*, *113*(G2), G02028. https://doi.org/10.1029/2007JG000635

Gharesifard, M., Wehn, U., & van der Zaag, P. (2017). Towards benchmarking citizen observatories: Features and functioning of online amateur weather networks. *Journal of Environmental Management*, *193*, 381–393. https://doi.org/10.1016/j.jenvman.2017.02.003

Giacomelli, A., Bacchiega, U., Troch, P. A., & Mancini, M. (1995). Evaluation of surface soil moisture distribution by means of SAR remote sensing techniques and conceptual hydrological modelling. *Journal of Hydrology*, *166*(3–4), 445–459. https://doi.org/10.1016/0022-1694(94)05100-C

Gower, S. T., Kucharik, C. J., & Norman, J. M. (1999). Direct and indirect estimation of leaf area index, fAPAR, and net primary production of terrestrial ecosystems. *Remote Sensing of Environment*, *70*(1), 29–51. http://dx.doi.org/10.1016/S0034-4257(99)00056-51

Gutman, G., & Ignatov, A. (1998). The derivation of the green vegetation fraction from NOAA/AVHRR data for use in numerical weather prediction models. *International Journal of Remote Sensing*, *19*(8), 1533–1543. https://doi.org/10.1080/014311698215333

Hadj-Hammou, J., Loiselle, S., Ophof, D., & Thornhill, I. (2017). Getting the full picture: Assessing the complementarity of citizen science and agency monitoring data. *PLoS One*, *12*(12), 1–18. https://doi.org/10.1371/journal.pone.0188507

Huete, A. R. (1988). A Soil-Adjusted Vegetation Index (SAVI). *Remote Sensing of Environment*, *25*(3), 295–309. https://doi.org/10.1016/0034-4257(88)90106-X

Jimenez-Munoz, J. C., Sobrino, J. A., Skokovic, D., Mattar, C., & Cristobal, J. (2014). Land surface temperature retrieval methods from Landsat-8 thermal infrared sensor data. *IEEE Geoscience and Remote Sensing Letters*, *11*(10), 1840–1843. https://doi.org/10.1109/LGRS.2014.2312032

Kenawy, A. M., & McCabe, M. F. (2016). A multi-decadal assessment of the performance of gauge- and model-based rainfall products over Saudi Arabia: Climatology, anomalies and trends. *International Journal of Climatology*, *36*(2), 656–674. https://doi.org/10.1002/joc.4374

Kerr, Y. H., Waldteufel, P., Wigneron, J.-P., Delwart, S., Cabot, F., Boutin, J., Escorihuela, M.-J., Font, J., Reul, N., Gruhier, C. (2010). The SMOS mission: New tool for monitoring key elements of the global water cycle. *Proceedings of the IEEE*, *98*(5), 666–687. https://doi.org/10.1109/JPROC.2010.2043032.

Kovács, K. Z., Hemment, D., Woods, M., van der Velden, N. K., Xaver, A., Giesen, R. H., Burton, V. J., Garrett, N. L., Zappa, L., Pelloquin, C., Long, D., Dobos, E., & Skalsky, R. (2019). Citizen observatory based soil moisture monitoring – The GROW example. *Hungarian Geographical Bulletin*, *68*(2), 119–139. https://doi.org/10.15201/hungeobull.68.2.2

Kutílek, M., & Nielsen, D. R. (1994). *Soil hydrology* (pp. 370). Catena *Verlag*.

Mazzoleni, M., Verlaan, M., Alfonso, L., Monego, M., Norbiato, D., Ferri, M., & Solomatine, D. P. (2017). Can assimilation of crowdsourced data in hydrological modelling improve flood prediction? *Hydrology and Earth System Sciences*, *21*(2), 839–861. https://doi.org/10.5194/hess-21-839-2017

Michael, P. R., Johnston, D. E., & Moreno, W. (2020). A conversion guide: Solar irradiance and lux illuminance. *Journal of Measurements in Engineering*, *8* (4), 153–166. https://doi.org/10.21595/jme.2020.21667

Michels, M., Fecke, W., Feil, J. H., Musshoff, O., Pigisch, J., & Krone, S. (2020). Smartphone adoption and use in agriculture: Empirical evidence from Germany. *Precision Agriculture*, *21*(2), 403–425. https://doi.org/10.1007/s11119-019-09675-5

Mishra, A. K., & Coulibaly, P. (2009). Developments in hydrometric network design: A review. *Reviews of Geophysics*, *47*(2), RG2001. https://doi.org/10.1029/2007RG000243

Nilson, T. (1971). A theoretical analysis of the frequency of gaps in plant stands. *Agricultural Meteorology*, *8*, 25–38. https://doi.org/10.1016/0002-1571(71)90092-6

Ochoa-Tocachi, W., Buytaert, J., Antiporta, L., Acosta, J. D., Bardales, R., Célleri, P., & Viñas, B. D. Bièvre (2018). High-resolution hydrometeorological data from a network of headwater catchments in the tropical Andes. *Science Data*, *5*(1), 180080. https://doi.org/10.1038/sdata.2018.80

Oki, T., & Kanae, S. (2006). Global hydrological cycles and world water resources. *Science*, *313*(5790), 1068–1072. https://doi.org/10.1126/science.1128845

Panjabi, K., Rudra, R., Gregori, S., Goel, P., Daggupati, P., Shukla, R., & Mekonnen, B. (2018). Development and field evaluation of a low-cost wireless sensor network system for hydrological monitoring of a small agricultural watershed. *Open Journal of Civil Engineering*, *8*(2), 166–182. https://doi.org/10.4236/ojce.2018.82014

Parlange, M. B., Albertson, J. D., Eichinger, W. E., Cahill, A. T., & Jackson, T. J. (1999). Evaporation: Use of fast response turbulence sensors, Raman lidar and passive microwave remote sensing. In M. B. Parlange & J.W. Hopmans (Eds.), *Vadose zone hydrology: Cutting across disciplines*, Oxford UniversityPress (pp. 260–278).

Phillips, A. J., Newlands, N. K., Liang, S. H. L., & Ellert, B. H. (2014). Integrated sensing of soil moisture at the field-scale: Measuring, modeling and sharing for improved agricultural decision support. *Computers and Electronics in Agriculture*, *107*, 73–88. https://doi.org/10.1016/j.compag.2014.02.011

Pocock, M. J. O., Tweddle, J. C., Savage, J., Robinson, L. D., & Roy, H. E. (2017). The diversity and evolution of ecological and environmental citizen science. *PLoS ONE*, *12*(4), e0172579. https://doi.org/10.1371/journal.pone.0172579

Priestley, C., & Taylor, R. J. (1972). On the assessment of surface heat flux and evaporation using large-scale parameters. *Monthly Weather Review*, *100*(2), 81–92. https://doi.org/10.1175/1520-0493(1972)100<0081:OTAOSH>2.3.CO;2

Ramadan, M. K., Oates, M. J., Molina-Martinez, J. M., & Ruiz-Canales, A. (2018). Design and implementation of a low cost photovoltaic soil moisture monitoring station for irrigation scheduling with different frequency domain analysis probe structures. *Computers and Electronics in Agriculture*, *148*, 148–159. https://doi.org/10.1016/j.compag.2017.12.038

Skokovic, D., Sobrino, J. A., & Jimenez-Munoz, J. C. (2017a). Vicarious calibration of the Landsat 7 thermal infrared band and LST algorithm validation of the ETM+ instrument using three global atmospheric profiles. *IEEE Transactions on Geoscience and Remote Sensing*, *55*(3), 1804–1811. https://doi.org/10.1109/TGRS.2016.2633810

Skokovic, D. (2017b). Calibration and Validation of Thermal Infrared Remote Sensing Sensors and Land/Sea Surface Temperature Algorithms over the Iberian Peninsula. Ph.D. Thesis, Universidad de Valencia.

Sliney, D. H. (2007). Radiometric quantities and units used in photobiology and photochemistry: Recommendations of the commission internationale de l'eclairage (international commission on illumination). *Photochemistry and Photobiology*, *83*(2), 425–432. https://doi.org/10.1562/2006-11-14-RA-1081

Sobrino, J. A., Jimenez-Muoz, J. C., Soria, G., Romaguera, M., Guanter, L., Moreno, J., Plaza, A., & Martinez, P. (2008). Land surface emissivity retrieval from di_erent VNIR and TIR sensors. *IEEE Transactions on Geoscience and Remote Sensing*, *46*(2), 316–327. https://doi.org/10.1109/TGRS.2007.904834

Sun, C., & Ren, L. (2014). Assessing crop yield and crop water productivity and optimizing irrigation scheduling of winter wheat and summer maize in the Haihe plain using SWAT model. *Hydrological Processes*, *28* (4), 2478–2498. https://doi.org/10.1002/hyp.9759

Tagarakis, A. C., Kateris, D., Berruto, R., & Bochtis, D. (2021). Low-cost wireless sensing system for precision agriculture applications in orchards. *Applied Science*, *11* (13), 5858. https://doi.org/10.3390/app11135858

Vellidis, G., Liakos, V., Andreis, J. H., Perry, C. D., Porter, W. M., Barnes, E. M., & Migliaccio, K. W. (2016). Development and assessment of a smartphone application for irrigation scheduling in cotton. *Computers and Electronics in Agriculture*, *127*, 249–259. https://doi.org/10.1016/j.compag.2016.06.021.

Vermote, E. F., Tanré, D., Deuzé, J. L., Herman, M., & Morcrette, -J.-J. (1997). Second simulation of the satellite signal in the solar spectrum, 6S: An overview. *IEEE Transactions on Geoscience and Remote Sensing*, *35*(3), 675–686. https://doi.org/10.1109/36.581987

Watson, D. J. (1947). Comparative physiological studies in the growth of field crops. I. Variation in net assimilation rate and leaf area between species and varieties, and within and between years. *Annals of Botany*, *11*(1), 41–76. https://doi.org/10.1093/oxfordjournals.aob.a083148

Woods, M., Hemment, D., Ajates, R., Cobley, A., Xaver, A., & Konstantakopoulos, G. (2020). GROW Citizens' observatory: Leveraging the power of citizens, open data and technology to generate engagement, and action on soil

policy and soil moisture monitoring. *IOP Conference Series: Earth Environment Science*, 509 012060. https://doi.org/10.1088/1755-1315/509/1/012060.

Xaver, A., Zappa, L., Rab, G., Pfeil, I., Vreugdenhil, M., Hemment, D., & Dorigo, W. A. (2020). Evaluating the suitability of the consumer low-cost parrot flower power soil moisture sensor for scientific environmental applications. *Geoscientific Instrumentation, Methods and Data Systems*, *9*(1), 117–139. https://doi.org/10.5194/gi-9-117-2020

Yang, X., Shu, L., Chen, J., Ferrag, M. A., Wu, J., Nurellari, E., & Huang, K. (2021). A survey on smart agriculture: Development modes, technologies, and security and privacy challenges. *IEEE/CAA Journal of Automatica Sinica*, *8*(2), 273–302. https://doi.org/10.1109/JAS.2020.1003536

Zappa, L., Forkel, M., Xaver, A., & Dorigo, W. (2019). Deriving field scale soil moisture from satellite observations and ground measurements in a hilly agricultural region. *Remote Sensing*, *11*(22), 2596. https://doi.org/10.3390/rs11222596

Zucaro, R. (2014). Condizionalità Ex-Ante per le Risorse Idriche: Opportunità e Vincoli per il Mondo Agricolo. 120, Rome, INEA Istituto Nazionale di Economia Agraria. ISBN 978-88-8145-402-0